

Measuring chaos in string scattering processes

Massimo Bianchi^{1,2,*} Maurizio Firrotta^{1,2,†} Jacob Sonnenschein^{3,‡} and Dorin Weissman^{4,||}

¹*Dipartimento di Fisica, Università di Roma Tor Vergata,
Via della Ricerca Scientifica 1, 00133 Rome, Italy*

²*INFN sezione di Roma Tor Vergata Via della Ricerca Scientifica 1, 00133 Rome, Italy*

³*The Raymond and Beverly Sackler School of Physics and Astronomy, Tel Aviv University,
Ramat Aviv 69978, Tel Aviv, Israel*

⁴*Asia Pacific Center for Theoretical Physics, Pohang 37673, Republic of Korea*



(Received 15 June 2023; accepted 19 August 2023; published 7 September 2023)

We analyze the amplitudes of one highly excited string (HES) state with two or three tachyons in open bosonic string theory. We argue that these processes are chaotic by showing that the spacing ratios of successive peaks in the angular dependence of the amplitudes are distributed as predicted by the β -ensemble of random matrix theory (RMT). We show how the continuous parameter β depends on the level and helicity of the scattered HES state. We derive the scattering amplitude of an HES and three tachyons and show that it takes the form of the Veneziano amplitude times a dressing factor, and that the dressing is chaotic as a function of the scattering angle, in the sense that its spacing ratios match with RMT predictions.

DOI: [10.1103/PhysRevD.108.066006](https://doi.org/10.1103/PhysRevD.108.066006)

I. INTRODUCTION

Chaotic processes are common in a wide range of domains from physics, chemistry, and biology, to sociology and more. In physics they appear both in classical and in quantum phenomena, both for single-body and for many-body systems.

Several definitions and measures have been proposed in the analysis of chaos. In the context of quantum Hamiltonian systems one time-tested method is to compare the statistics of the energy spectrum to the predictions of random matrix theory (RMT), namely, to matrices whose elements are randomly chosen from a (usually Gaussian) random distribution (see [1,2] and many references therein). This correspondence was verified for single-particle systems as well as for many-body systems. Most of the latter models were discrete ones and only recently studies of continuous systems, and in particular quantum field theory (QFT), have been performed [3]. The toolkit for analyzing QFT models is not yet complete and

devising new and efficient measures is an important task in the field.

Recently in [4], motivated by [5], we proposed a novel measure for quantum scattering processes. The crucial idea was to relate the angular distribution of scattering amplitudes to the spectral statistics of quantum systems governed by RMT. We believe that this measure could be applied on any quantum amplitude given by an S -matrix.

In [4] we applied it in particular to scattering on a leaky torus [6] and to the decay of highly excited string (HES) states into two tachyons. A comparison was made against the “prototype” of quantum chaos that is the distribution of nontrivial zeros of the Riemann zeta function [7,8].

It is very natural to suspect that not only the decays of HES states, but the scattering processes of such states admit chaotic behavior as well. This study was initiated in [5,9,10], where scattering amplitudes involving three or four external legs were analyzed and were shown to display erratic behavior. In particular a drastic difference was observed in the scattering amplitudes where the scattered HES state is changed in a minor way in its structure. However, the authors of [5,9,10] did not directly quantify these type of differences. The measure that we proposed in [4] was introduced to fulfill this purpose. Indeed it allowed us to demonstrate that decays of HES states into two tachyons did admit a chaotic behavior.

The goal of this paper is to expand on the results of [4] and to apply the method also to four-point scattering amplitudes involving an HES state. Chaotic scattering of HES states is especially interesting because of the proposed

*massimo.bianchi@roma2.infn.it

†maurizio.firrotta@gmail.com

‡cobi@tauex.tau.ac.il

||dorin.weissman@apctp.org

Published by the American Physical Society under the terms of the Creative Commons Attribution 4.0 International license. Further distribution of this work must maintain attribution to the author(s) and the published article's title, journal citation, and DOI. Funded by SCOAP³.

correspondence with black holes [11,12]. Determining chaotic patterns of string scattering together with the knowledge about the chaotic nature of black holes, may shed new light on the string/black hole correspondence.

Let us briefly review the relation of the spectral structure of a Hamiltonian system with eigenvalues E_n and RMT. Consider the spacings between eigenvalues [13],

$$\delta_n = E_{n+1} - E_n \quad (1.1)$$

and define the *ratios of successive spacings*

$$r_n \equiv \frac{E_{n+1} - E_n}{E_n - E_{n-1}} = \frac{\delta_{n+1}}{\delta_n}. \quad (1.2)$$

In chaotic systems the level spacings are distributed as the spacings of eigenvalues of random matrices. In order to see this one must first “unfold” the spectrum [14], to account for the average density of states and expose the erratic fluctuations. The related distribution function for r_n , as a ratio of nearby spacings is not very sensitive to the unfolding procedure and as such can be used directly on the spectrum. Distributions of these spacing ratios has been successfully used as a measure of chaos in works such as [3,15]. In some cases the normalized ratios $\tilde{r}_n \equiv \min\{r_n, \frac{1}{r_n}\}$, defined to be between 0 and 1, are used.

In analogy to the energy spacings, we proposed in [4] to analyze the spacings between successive peaks of a scattering amplitude $\mathcal{A}(\alpha)$ as a function of a continuous kinematical variable α , relevant to the scattering process under scrutiny. As for the energy spacings, we define the spacings δ_n between successive peaks and their ratios r_n , and compare the resulting distribution to RMT predictions.

Our analysis of the chaotic behavior of decays and scattering processes involving HES states can be divided in three steps. First, we construct the HES state in the DDF approach (after Del Giudice, Di Vecchia, and Fubini) [16].¹ In the second step we compute the relevant decay and scattering amplitudes as a function of the available kinematical variables. In this paper, this is done for a decay of an HES state into two tachyons and for the four point amplitude of an HES state and three tachyons. In both cases the amplitude is analyzed as a function of an angle. In the former case the angle is the difference between the emission angle of the outgoing tachyons and the momentum of the photons used to create the DDF state. In the latter it is the usual scattering angle in the $2 \rightarrow 2$ process. The third step is to determine the locations of the maxima of the amplitudes, then compute the adjacent spacings and their ratios. We then perform a statistical analysis of the probability distribution function of the ratios for various levels N and spin/helicity J of the HES state. This is fitted to the predicted distribution of

r_n from the Gaussian β -ensemble [25], in which β is a continuous variable interpolating between the classical Gaussian ensembles—orthogonal (GOE), unitary (GUE) and symplectic (GSE)—of RMT.

The results of our analysis are the following:

- (i) For the decay processes we find that the distribution of spacings of peaks of the amplitude is well modeled by the RMT formula of the β -ensemble, with the parameter β depending on the level N and the helicity J of the HES state. In the range of $N = 50$ –1600, we find that β is decreasing from 3.4 to around 1.7. This is also observed as a slow monotonous increase of the measured average $\langle r_n \rangle$ as a function of N .
- (ii) For the four-point scattering amplitude, we show that the amplitude is given by the Veneziano amplitude times a chaotic dressing factor which depends on the HES state. We analyze these dressing factors in the high-energy fixed-angle limit and the Regge limit, for HES states with $N = 100$ and find similar distributions for their r_n with values of β around 2 (the GUE value).
- (iii) In some cases, one can see clearly a transition from chaotic to regular spacings as one moves from small to large scattering angles.
- (iv) The chaotic behavior is observed for generic HES states, but it completely disappears for for states in the leading Regge trajectory or nearby states, i.e., for states with $N \approx J$.

The paper is organized as follows. After this introduction, in Sec. II we present and discuss measures of chaos in quantum scattering amplitudes. In particular we describe the novel measure that we have proposed in [4] and mention certain generalizations. In Sec. III we briefly review the β -ensemble of random matrices, including its Coulomb gas description. Section IV is devoted to a review of highly excited string states. We describe the construction of HES states using DDF operators and discuss integer partitions and the role of the helicity J . We then study the chaotic behavior of the decay of these highly excited states in Sec. V. We write down the decay amplitude of an HES to two tachyons and perform a statistical analysis of the relevant spacing ratios. This includes specifying a prescription of selection of the states and the fitting model. We then present the result of this analysis. Section VI is devoted to chaotic four-point scattering process involving one HES and three tachyons. The scattering amplitude of these processes is derived and written down. The amplitude is then analyzed in the high-energy fixed-angle regime and the Regge limit. We determine the spacing ratios for the four-point scattering amplitude, and describe the chaotic behavior in the two high-energy limits. We summarize the paper and mention several open questions in Sec. VII.

For the benefit of the reader we add four appendixes. In Appendix A we describe the kinematics of the four-point

¹See also [17–24] for more recent reviews and other applications.

amplitude at hand. We then present a derivation of the HES-three tachyon amplitude in Appendix B. In Appendix C we make an explicit comparison of the *beta*-ensemble with the log-normal distribution of r_n which we utilized as our main fitting model in our previous work [4]. Random partitions of a large-integer N are discussed in Appendix D.

II. MEASURE OF CHAOS FOR QUANTUM SCATTERING AMPLITUDES

Quantum scattering processes are characterized by a scattering amplitude. Suppose first that the scattering amplitude is a function of a scattering angle α , i.e., of a single continuous real parameter.

In analogy to energy-level spacings and their ratios, we propose to analyze a scattering amplitude $\mathcal{A}(\alpha)$ as a function of a scattering angle α as follows. In our case the “eigenvalues” would be the positions of local maxima and/or minima of the amplitude. We usually utilize the logarithmic derivative

$$F(\alpha) \equiv \frac{d}{d\alpha} \log \mathcal{A} \quad (2.1)$$

to find them. Then, our discrete levels are given by the set of zeros of $F(\alpha)$ in the range $(0, 2\pi)$,²

$$F(z_n) = 0. \quad (2.2)$$

Then we define, as for the energy levels, the spacings δ_n and the ratios of consecutive spacings, r_n and \tilde{r}_n ,

$$\delta_n = z_n - z_{n+1} \quad (2.3)$$

and

$$r_n \equiv \frac{z_{n+1} - z_n}{z_n - z_{n-1}} = \frac{\delta_{n+1}}{\delta_n}, \quad \tilde{r}_n = \min \left\{ r_n, \frac{1}{r_n} \right\}. \quad (2.4)$$

As mentioned in the introduction, when comparing level spacings to the predictions of random matrix theory, one typically has to perform an unfolding of the spectrum. A prototypical and useful example which we discussed in some detail in [4] is the distribution of spacings of non-trivial zeros of the Riemann zeta function. In that case, the z_n are the solutions of $F(z_n) = \zeta(\frac{1}{2} + iz_n) = 0$. There are infinitely many solutions, but one can consider finite subsets of them by limiting the range of z_n . Then, the normalized spacings $\tilde{\delta}_n = (z_n - z_{n-1}) \frac{\log(z_n/2\pi)}{2\pi}$ are known to match almost exactly with the distribution of spacings in the Gaussian unitary ensemble. In this case the formula for unfolding is known explicitly, but one could start with r_n as

defined above to see the agreement with the GUE without normalizing the spacings, since the logarithmic dependence in $\tilde{\delta}_n$ is slow enough such that $r_n \approx \tilde{\delta}_{n+1}/\tilde{\delta}_n$. In many practical applications, unfolding is done by fitting the average density to a polynomial rather than a logarithm. Still, as long as this function is slowly varying at the scale of the spacings, the distribution of r_n is only weakly affected by the unfolding procedure.

A generic scattering amplitude would depend on several kinematic variables like the incoming scattering angle, impact parameters, momenta, etc. In particular, a $2 \rightarrow 2$ scattering amplitude can be written as a function of two independent Mandelstam variables s and t , or alternatively as a function of s and one scattering angle, which is a simple function of the ratio t/s . Regardless of the parametrization, if we find an appropriate continuous variable α and function $F(\alpha)$ which appears erratic, we can analyze the spacings between zeros of $F(\alpha)$. If we can unfold the resulting “spectrum”, or simply use the ratios r_n , then we should not be too sensitive to the choice of variable and be able to compare with the predictions of RMT.

We can also generalize to a higher-dimensional version where the scattering depends on several continuous variables, which we can denote generically as $\alpha^{(i)}$. In a similar way, one can define $F(z_n^{(i)}) = 0$ and analyze the spacing vectors $\delta_n^i = z_n^i - z_{n+1}^i$. In the following, we will focus only on the dependence on a single kinematical variable. For the four-point scattering amplitude, as we will see, we will compute only chaotic behavior in the scattering angle θ when s is large and fixed.

We now review the statistical distributions for the spacings and their ratios associated to random matrices.

III. THE β -ENSEMBLE OF RANDOM MATRICES

A. Distributions of eigenvalue spacings and their ratios

The three classical Gaussian ensembles of random matrix theory [1,2] are the Gaussian orthogonal ensemble, the Gaussian unitary ensemble, and the Gaussian symplectic ensemble. The eigenvalues of $N \times N$ matrices in these ensembles have the joint probability density function (PDF) which is

$$P_N(\lambda_1, \lambda_2, \dots, \lambda_N) = C(\beta) \times \exp \left(-\frac{\beta}{2} \sum_{i=1}^N \lambda_i^2 \right) \prod_{1 \leq i < j \leq N} |\lambda_i - \lambda_j|^\beta, \quad (3.1)$$

where $\beta = 1, 2$, or 4 for the GOE, GUE, and GSE, respectively, and $C(\beta)$ is a normalization constant. One can generalize from these three special cases by taking β to be a continuous parameter, and defining in this way the β -ensemble for any $\beta > 0$ starting from the above distribution.

²Symmetries of the amplitude in the angle would allow us to eventually reduce the range to $(0, \pi/2)$.

One of the main objects of study in a given system are its level spacings. The distributions for the difference of eigenvalues $\delta = \lambda_2 - \lambda_1$ of a 2×2 matrix of the ensemble, properly normalized such that $\langle \delta \rangle = 1$, are given by the well-known Wigner surmises,

$$p_\beta(\delta) = \mathcal{N}_\beta \delta^\beta \exp(-c_\beta \delta^2) \quad (3.2)$$

with

$$\mathcal{N}_\beta = 2 \frac{[\Gamma(\frac{\beta+2}{2})]^{\beta+1}}{[\Gamma(\frac{\beta+1}{2})]^{\beta+2}}, \quad c_\beta = \left(\frac{\Gamma(\frac{\beta+2}{2})}{\Gamma(\frac{\beta+1}{2})} \right)^2. \quad (3.3)$$

Rather than the spacings themselves, we will focus on the ratios of consecutive spacings. In the minimal case of a 3×3 matrix with eigenvalues $\lambda_1 < \lambda_2 < \lambda_3$, the PDF of the ratio $r = (\lambda_3 - \lambda_2)/(\lambda_2 - \lambda_1)$ in the β -ensemble is [25]

$$f_\beta(r) = \frac{3^{\frac{3+\beta}{2}} \Gamma(1 + \frac{\beta}{2})^2}{2\pi \Gamma(1 + \beta)} \frac{(r + r^2)^\beta}{(1 + r + r^2)^{1 + \frac{3+\beta}{2}}}. \quad (3.4)$$

The distribution is symmetric under $r \rightarrow \frac{1}{r}$ since

$$f_\beta(r) = \frac{1}{r^2} f_\beta\left(\frac{1}{r}\right). \quad (3.5)$$

For larger $N \times N$ matrices it is shown numerically that the deviations from the distributions (3.2) and (3.4) are small. An explicit comparison can be found in [25] where finite size random matrices and exact results for large N size are shown to agree up to negligible corrections.

Equation (3.4) will be our main fitting model for the distribution of spacing ratios in string scattering amplitudes. We will also consider the variable $\tilde{r} \equiv \min(r, \frac{1}{r})$. Thanks to the symmetry property of $r \rightarrow 1/r$, the PDF of \tilde{r} is simplify $2f_\beta(\tilde{r})$ restricted to the range $\tilde{r} \in [0, 1]$.

For large matrix sizes, the formulas for level spacings and spacing ratios are also applicable to the spacings of the phases of eigenvalues of the circular ensembles of random unitary matrices, being the circular orthogonal (COE), unitary (CUE), and symplectic (CSE) ensembles [1].

B. Log-gases and the β -ensemble

A physical system described by the β -ensemble is the log-gas [26,27], a Coulomb gas of N charged particles interacting through a logarithmic potential between each pair,

$$V_{ij}(x_i, x_j) = \log |x_i - x_j|. \quad (3.6)$$

For our purposes, the system is taken to be one dimensional.

In addition to the pairwise interaction one should introduce a background charge density $\rho_0(x)$ such that

the total charge is zero. The neutrality condition is that $\int dx \rho_0(x) = -N$, since each particle is taken to have unit charge. The interaction of the background charge density with the i th charge contributes a term

$$V_i(x_i) = \int dx' \log |x - x'| \rho_0(x') \quad (3.7)$$

to the total potential.

Now, taking a charge density confined to the interval $(-\sqrt{2N}, \sqrt{2N})$ and of the form

$$\rho_0(x) = -\frac{\sqrt{2N}}{\pi} \sqrt{1 - \frac{x^2}{2N}} \quad (3.8)$$

one finds that, up to a constant, $V_i(x) = -\frac{x^2}{2}$. The full potential is

$$V(x_1, \dots, x_N) = \text{Const} - \sum_{i=1}^N \frac{x_i^2}{2} + \sum_{1 \leq i < j \leq N} \log |x_i - x_j|. \quad (3.9)$$

Then, one can see that, for a given ‘‘microstate’’ corresponding to a choice of (x_1, x_2, \dots, x_N) , the Boltzmann factor $e^{-\beta V(x_1, \dots, x_N)}$ takes exactly the form of Eq. (3.1), with β precisely identified with the inverse temperature of the gas.³

IV. HIGHLY EXCITED STRING STATES

A. Regge resonances and DDF operators

The string spectrum contains an infinite number of massive higher-spin excitations often called Regge resonances. They lie on linear Regge trajectories in the plane (J, M^2) with Regge slope α' and an intercept that depends on the model. For the open bosonic strings that we focus on the spectrum is given by

$$\alpha' M^2 = N - 1, \quad (4.1)$$

where $N = \sum_n n g_n$ is the ‘‘level’’ and $J = \sum_{n=1} g_n \leq N$ is the helicity of the string state, assuming only transverse oscillators are taken into account.

The lowest-lying states are easy to characterize. The ground state $N = 0$ is a scalar tachyon with $J = 0$ and $\alpha' M^2 = -1$. The first excited state $N = 1$ is a massless vector boson ($J = 1, \alpha' M^2 = 0$). The first massive (second excited) level $N = 2$ is a massive tensor boson made up of two terms, $J = 2 = g_1$ and $J = 1 = g_2$, such that $\alpha' M^2 = 1 = (1 + 1) - 1 = 2 - 1$. Note that the $J = 1$ transverse ‘‘vector’’ polarizations are those needed to make

³The Coulomb gas representation corresponding to a logarithmic potential finds many applications in 2D – CFT including minimal models, Liouville models and many others [28–30].

the helicity $J = 2$ states massive (the latter comprise a $J = 0$ state related to the “trace” over the transverse indices, i.e., their contractions).

The situation soon becomes very messy since the degeneracy of the states with the level grows (for large N and up to a constant) as

$$d_N \simeq N^{-\frac{c+3}{4}} \exp\left(2\pi\sqrt{\frac{c}{6}N}\right) \\ = N^{-\frac{27}{4}} \exp(4\pi\sqrt{N}) \quad \text{for } c = c_t = 24 = 26 - 2 \quad (4.2)$$

which counts the partitions of the integer N , encoded in Dedekind η function

$$\mathcal{Z}_B(q) = \frac{1}{\eta(q)^{24}} = \frac{1}{q \prod_{n=1}^{\infty} (1 - q^n)^{24}} \\ = \frac{1}{q} \left(\sum_k d_k q^k \right)^{24}. \quad (4.3)$$

The situation drastically simplifies for the first Regge trajectory with $J = N$, i.e., for the states with maximal spin at a given level. These correspond to $g_1 = N$ and all the other $g_k = 0$ for $k > 1$.

Counting states with a given spin S at level N is quite involved. One starts with the multihelicity (super)trace

$$\mathcal{B}(q, \alpha_I) = \frac{1}{q \prod_{I=1}^{12} \prod_{n=1}^{\infty} (1 - e^{i\alpha_I} q^n) (1 - e^{-i\alpha_I} q^n)} \quad (4.4)$$

and then expands in characters of $SO(24)$. Setting $\alpha_I = \alpha$ for all $I = 1, \dots, 12$ counts the total “helicity” J , which is less than the full actual “spin”, $J \leq S \leq S_{\text{Max}} = N$, where S is what classifies the representations of $SO(25)$. In fact tensors with mixed symmetry can appear for which the notion of spin is not even well-defined.

If one focuses on three spatial directions the situation improves since one can put $\alpha_1 = \alpha$ and all the rest to zero, $\alpha_I = 0$ for $I = 2, \dots, 12$. The relevant characters of $SU(2) \sim SO(3) \supset SO(2)_T$ are identical to the Gegenbauer polynomials of parameter 1^4

$$\mathcal{X}_J(\alpha) = \sum_{m=-J}^{m=J} e^{iam} = \frac{\sin(2J+1)\frac{\alpha}{2}}{\sin\frac{\alpha}{2}}. \quad (4.5)$$

Using orthogonality of the characters

$$\mathcal{B}(q, \alpha_1, \alpha_{I \neq 1} = 0) = \frac{1}{q} \sum_N d_N(J) q^N \mathcal{X}_J(\alpha) \quad (4.6)$$

one has

⁴These are relevant in the scattering in $D = 5$ as in [31,32].

$$d_N(J) = \oint \frac{dq}{q^N} \int \frac{d\alpha}{2\pi} \mathcal{X}_J(\alpha) \mathcal{B}(q, \alpha_1, \alpha_{I \neq 1} = 0). \quad (4.7)$$

Later on we will give an estimate of $d(N, J)$.

Let us consider other physical properties of HES states. Regge resonances are very narrow (zero width) for string coupling $g_s = 0$ (free string) but acquire a finite width when $g_s \neq 0$. To lowest order in g_s , their decay amplitude corresponds to a 3-point function on the disk

$$\mathcal{A}(p_1, p_2, p_3) = \langle V(p_1, H_1) V(p_2, H_2) V(p_3, H_3) \rangle, \quad (4.8)$$

where V is a Becchi-Rouet-Stora-Tyutin (BRST) invariant vertex operator with momentum p and “polarization” H . Let us focus on the decay amplitude of a massive higher-spin state at level N into two tachyons.

While the BRST invariant vertex operator for a tachyon is simply

$$V_T = e^{ipX} \quad (4.9)$$

with $p^2 = -M^2 = 1/\alpha'$, writing down the most general “covariant” vertex operator for massive states is very challenging due to the large “gauge symmetry”. The problem can be overcome by relying on the time-honored DDF approach [16].

The DDF construction is based on the choice of an arbitrary tachyonic momentum p ($p^2 = 1/\alpha'$) and a null momentum q ($q^2 = 0$) chosen in such a way that $2\alpha' p \cdot q = -1$. A massive on-shell momentum at level N obtains

$$p_N = p - Nq, \quad (4.10)$$

that suggests a physical interpretation of the excited string state as the tachyonic state with momentum p that successively emits (absorbs) massless vector bosons with momentum q ($-q$). See Fig. 1 for a pictorial representation. With a choice of q one can define the DDF operators

$$A_n^i(q) = \oint \frac{dz}{2\pi} \partial X^i e^{inqX}, \quad (4.11)$$

where i runs over the transverse directions, i.e., $q \cdot A = 0$. The most general BRST invariant state can be written as

$$|\{g_n\} : N = \sum_n n g_n, p_N = p - Nq \rangle = \prod_{n=1}^{\infty} A_{-n}^i(q) |0, p\rangle. \quad (4.12)$$

For simplicity let us focus on the level N states of the form

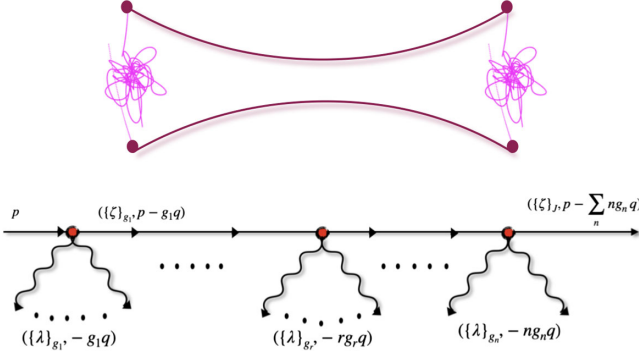


FIG. 1. Above: a representation of the profile of a generic highly excited open string state, where the magenta lines describe the complexity of the profile. Below: the DDF construction of such state. We start from a tachyonic vacuum state with momentum p and we use the iterative action (codified in the operator product expansion represented by the red points) of DDF creation operators (which are described by the photon lines with polarizations $\{\lambda\}$ and momentum $-ng_n q$). We end up with a final state $H_N^{(i)}(\{\zeta\}; p_N)$ with final momentum $p_N = p - q \sum_n n g_n$ and polarizations $\{\zeta\}$, as in Eq. (4.13).

$$\prod_{n=1}^{\infty} (\lambda \cdot A_{-n}(q))^{g_n} |0, p\rangle = |H_N^{(i)}(\{\zeta\})\rangle, \quad (4.13)$$

where λ is a complex transverse (“null” in the sense that $\lambda \cdot \lambda = 0$) vector polarization and $\zeta = \lambda - 2\alpha'(\lambda \cdot p)q$ such that $p \cdot \zeta = q \cdot \zeta = 0$. For this state we can compute for instance its decay amplitude into two tachyons with momenta p_1 and p_2 with $p - Nq + p_1 + p_2 = 0$ for momentum conservation.

Moreover if the initial excited string state had definite spin \vec{S} (whichever the mass/level)⁵ the amplitude would simply be

$$\mathcal{A}_{HTT} = C_S^{(H)} H_S \cdot (\vec{p}_1 - \vec{p}_2)^{\otimes S} \quad (4.14)$$

so that the angular distribution of the products (tachyons) would be completely fixed to be the Legendre polynomial $P_S(\vec{n} \cdot \vec{n}_p)$ with $\vec{n}_p = \frac{\vec{p}_1 - \vec{p}_2}{|\vec{p}_1 - \vec{p}_2|}$ in the rest frame of the decaying particle, whereby $\vec{p}_2 = -\vec{p}_1$, while $|\vec{p}_1| = |\vec{p}_2| = \frac{1}{\alpha'} + \frac{M^2}{4}$.

This shows no chaotic behavior, for instance this would be the case for states of the first Regge trajectory. On the contrary using the exponential degeneracy at level N one can consider a generic state $H_N^{(i)}$ without definite helicity J or even with definite helicity but without definite spin S . This exposes chaotic behavior due to the random and highly erratic superposition of spin components in the

⁵Even superposition of mass eigenstates with different masses would give a ‘trivial’ angular distribution as long as all the spins are aligned, i.e., $\vec{J}_N = \vec{J}'_N$ in the superposition.

generic state. As shown in [9] the erratic behavior is exposed even for similar partitions.

Though the HES state we consider in (4.13) is quite generic it is not the most general one. We cannot exclude that this choice might introduce some biases in our analysis below of the chaotic behavior of processes involving these HES. The analysis of similar processes with the most general BRST invariant HES is much more involved and beyond the scope of the present investigation.

B. Integer partitions

Since our HES states are characterized by a choice of a partition of the level $N \sim M^2$, we discuss here some basic properties of integer partitions that will be useful in the following.

The state $H_N^{(i)}$ is a state constructed from the DDF operators with a particular choice of polarizations,

$$|H_N^{(i)}\rangle = \prod_{n=1}^N (\lambda \cdot A_n)^{g_n} |0\rangle \quad (4.15)$$

and is defined by the integer partition $\{g_n\}$ for which

$$N = \sum_{n=1}^{\infty} n g_n, \quad J = \sum_{n=1}^{\infty} g_n. \quad (4.16)$$

For fixed λ , the number of states of this form at level N is equal to the total number of integer partitions of N . In our notation (i) is an index enumerating the states at level N which needs no precise definition.

The total number of partitions of N into at most J summands can be computed from the generating function

$$F_J(x) = \sum_{N=1}^{\infty} C_{N,J} x^N = \prod_{k=1}^J \frac{1}{1-x^k} \quad (4.17)$$

and therefore the number of partitions of length exactly J is given by

$$p_{N,J} = C_{N,J} - C_{N,J-1}. \quad (4.18)$$

The total number of partitions of N is also given by the above generating function as $p_N = C_{N,N}$. The number of partitions behaves for large N as

$$p_N \approx \frac{1}{4\sqrt{3N}} e^{C\sqrt{N}}, \quad C \equiv \pi\sqrt{\frac{2}{3}}. \quad (4.19)$$

The number of partitions of fixed length J is asymptotically given by a Gumbel distribution [33], i.e., according to the probability density function

$$d_N(J) = \frac{1}{\nu} \exp\left(-\frac{J-\mu}{\nu} - e^{-\frac{J-\mu}{\nu}}\right) \quad (4.20)$$

with the parameters scaling as $\mu \sim \sqrt{N} \log N$ and $\nu \sim \sqrt{N}$. More specifically the distribution is centered around

$$\langle J \rangle \approx \frac{1}{C} \sqrt{N} \log N \quad (4.21)$$

which makes this the ‘‘typical helicity’’ of a randomly chosen string state at level N .

In addition to J another useful parameter of a given partition is n_{\max} , the largest summand in the partition, i.e., the largest n for which $g_n \neq 0$. It is easy to see that n_{\max} is exactly the length of the conjugate partition. The conjugation of integer partition is most easily understood as a rotation and reflection of the Ferrers diagram associated with the partition, exchanging rows for columns. For example

$$\begin{array}{ccc} 4 + 3 + 2 + 2 + 1 & & 5 + 4 + 2 + 1 \\ \bullet & & \bullet & & \bullet & & \bullet & & \bullet \\ \bullet & & \bullet & & \bullet & & \bullet & & \bullet \\ \bullet & & \bullet & & \bullet & & \bullet & & \bullet \\ \bullet & & \bullet & & \bullet & & \bullet & & \bullet \\ \bullet & & \bullet & & \bullet & & \bullet & & \bullet \\ \bullet & & \bullet & & \bullet & & \bullet & & \bullet \\ \bullet & & \bullet & & \bullet & & \bullet & & \bullet \end{array} \longleftrightarrow$$

are two partitions of 12, conjugate to each other. Since conjugation is a one-to-one operation, it follows immediately that the number of partitions of N into integers less or equal to n is the same as the number of partitions of length $J = n$. This is particularly useful for generating random partitions of fixed length, as described in Appendix D.

V. CHAOS IN THE DECAY AMPLITUDE OF A HIGHLY EXCITED STRING

A. The decay amplitude

We study the decay amplitude of a highly excited string state into two tachyons. The relevant kinematical variable is α , the angle between the outgoing tachyons and the photons used to create the DDF state, i.e., the angle between the momentum of one of the tachyons and the photon momentum q seen e.g., in Eq. (4.13).

The angular dependence of the full amplitude can be compactly written as [9]

$$\mathcal{A}_{H_N^{(i)} \rightarrow TT} \propto (\sin \alpha)^J \prod_{n=1}^N \left(\sin\left(\pi n \cos^2 \frac{\alpha}{2}\right) \frac{\Gamma(n \cos^2 \frac{\alpha}{2}) \Gamma(n \sin^2 \frac{\alpha}{2})}{\Gamma(n)} \right)^{g_n}, \quad (5.1)$$

where $H_N^{(i)}$ is a state defined by an integer partition $\{g_n\}$ of level N and with helicity J , as described in the previous section.

Another representation of the amplitude can be reached using basic identities of the gamma function, $\Gamma(z+1) = z\Gamma(z)$ and $\Gamma(z)\Gamma(1-z)\sin(\pi z) = \pi$. Then, each term in the product is a polynomial in $x \equiv \cos^2 \frac{\alpha}{2}$ of degree $m-1$, which can be written compactly using the Pochhammer symbol,

$$\begin{aligned} & \frac{\Gamma(n(1-x))\Gamma(nx)\sin(n\pi x)}{\Gamma(n)} \\ &= \frac{\pi}{(n-1)!} (1-nx)_{n-1} \\ &= \pi \left(1 - \frac{nx}{n-1}\right) \left(1 - \frac{nx}{n-2}\right) \dots \left(1 - \frac{nx}{1}\right) \end{aligned} \quad (5.2)$$

so that the amplitude is written most compactly as

$$\mathcal{A}_{H_N^{(i)} \rightarrow TT} \propto (\sin \alpha)^J \prod_{n=1}^N \left(\frac{(1 - n \cos^2 \frac{\alpha}{2})_{n-1}}{\Gamma(n)} \right)^{g_n}. \quad (5.3)$$

It is convenient for computation and visualization to work with the logarithmic derivative,

$$\begin{aligned} F(\alpha) &\equiv \frac{d}{d\alpha} \log \mathcal{A} \\ &= J \cot \alpha - \frac{1}{2} \sin \alpha \sum_{n=1}^N g_n \sum_{k=1}^{n-1} \frac{n}{n-k - n \cos^2 \frac{\alpha}{2}}. \end{aligned} \quad (5.4)$$

The points z_n at which $F(z_n) = 0$ are the local maxima and minima of $\mathcal{A}(\alpha)$, and they are always maxima of the absolute value $|\mathcal{A}|$. For this reason we can refer to all the extremal points of the amplitude collectively as its peaks.

In terms of $x = \cos^2 \frac{\alpha}{2}$, the peaks are located at the points where

$$\begin{aligned} F(x) &= \frac{1}{2\sqrt{x(1-x)}} \\ &\times \left(J(2x-1) - 2x(1-x) \sum_{n=1}^N g_n \sum_{k=1}^{n-1} \frac{n}{k-nx} \right) \\ &= 0 \end{aligned} \quad (5.5)$$

which is a polynomial equation in x .

Our object of study is the distribution of the ratios of the spacings between consecutive solutions of $F(\alpha) = 0$.

B. Statistical analysis of spacing ratios

Our main result is that the ratios r_n of the spacings between consecutive peaks of the amplitude (5.1) are distributed as predicted by the β -ensemble, i.e., as in the

distribution of Eq. (3.4), with β depending on the parameters of the HES state. In the following we describe in detail the statistical analysis that leads to this result.

1. Fitting model and selection of states

For a generic state at level N , the number of peaks in the decay amplitude (or zeros of its logarithmic derivative) scales linearly with N . For very large values of N , say $N \sim 10,000$, there would be sufficient zeros such that one could measure the distribution of spacing ratios in a single amplitude of a particular excited string state. For intermediate N , meaning of order 100, we collect data from many different states in order to perform the statistical analysis.

Denoting the set of ratios for a specific state $H_N^{(i)}$ as $\{r_n\}_{N^{(i)}}$, we will study the distribution of the values in the union of many such sets, which we can write as

$$\{r_n\}(\mathcal{S}) \equiv \bigcup_{N^{(i)} \in \mathcal{S}} \{r_n\}_{N^{(i)}} \quad (5.6)$$

for some specific sample subset of states \mathcal{S} .

Once we have a set of $\{r_n\}$ with enough data points, we fit their distribution to that of r in the β -ensemble of Eq. (3.4). There is a single continuous and positive fitting parameter, β , which can be directly related to the average value of the distribution $\langle r \rangle$. We will examine the behavior of the average $\langle r_n \rangle$ in detail in the following.

Since the space of all possible states is too large to study, we must choose wisely which states would go into a representative sample. We observe from the data that there is a dependence of $\langle r_n \rangle$ on the level number N and the helicity J . It is then assumed, as a model, that the fitting parameters depend only on N and J , though the full physical picture could be more complex.

There are some technical difficulties in selecting random states to go into a sample. Our aim is to choose “generic” states once we have fixed N and (optionally) J . The most straightforward way is to select at random a small sample from the full list of possible states, with each state having an equal probability of being chosen. At some point this becomes impractical as the list of possible states grows exponentially. It is nontrivial to devise an algorithm that will generate random partitions of a large integer in such a way that all partitions are equally likely to be chosen (see Appendix D for details). For our purposes it is important not to introduce any biases in the selection of states, since we cannot predict how that might affect the results. Once we fix the parameters, the selection will be random, with all partitions of the given N (and J when that is fixed) having equal probability to go into the sample. Our samples will typically consist of thousands of states, which will provide more than enough data to observe a distribution of the spacing ratios, but we keep in mind that the states in the sample still represent only an exponentially small fraction of the states of the highly excited string.

2. Results

The results of our analysis indicate that the distribution of spacings of peaks of the amplitude is well modeled by the random matrix formula of the β -ensemble, with the β parameter depending on the decaying state. Specifically we measure the dependence on the level N and the helicity J . The results are collected in Tables I–III.

In the present case we have analyzed states up to $N = 1600$. The results are generally well-fitted by the predicted distribution. There are some deviations, but these become small as we increase N , see Fig. 2.

We observe a monotonous increase of the average $\langle r_n \rangle$ with the level N . The growth appears to be logarithmic at most, and it is impossible to tell from the data whether it continues indefinitely as $N \rightarrow \infty$ or approaches some asymptotic value. In [4] we noted that there is a similar dependence of $\langle r_n \rangle$ when examining the spacings of the nontrivial zeros of the Riemann zeta function. There, the average increased slowly as one covered a larger and larger range of zeros, but it eventually approaches the value predicted from the GUE. The numerical evidence for this is very strong, thanks to the vast range of zeros of the zeta function that has been computed [34,35].

For reference, the predicted averages of $\langle r \rangle$ ($\langle \tilde{r} \rangle$) are, 1.75 (0.536) for GOE and 1.361 (0.603) for GUE. As a function of β , $\langle r \rangle$ is a monotonously decreasing function. It diverges at $\beta = 0$ and approaches 1 at large β . The average of $\langle \tilde{r} \rangle$ increases from ≈ 0.408 at $\beta = 0$ to 1 at large β .⁶

A question that one can ask is whether spacing ratios in the string amplitudes also approach the GUE distribution at very large N . This distribution is supported by the observations that the S -matrix is a unitary operator and that the HES we consider is a “random” superposition of states at level N related to one another by a unitary transformation.⁷ In fact the CUE that describes random unitary matrices with norm one eigenvalues $\lambda_k = e^{i\varphi_k}$ would look even more appropriate, given the unitarity of the scattering matrix and the fact that our eigenvalues are indeed angles. However, the distinction between CUE and GUE will not come into play here, since as mentioned above, it is known that for large matrices GUE and CUE distributions coincide insofar as the level spacings are concerned.

From Table I one can see that around $N = 200$ the best fit for β is close to the GUE value of 2, but as we increase N we reach $\beta < 2$. The deviation that we find at $N = 1600$, the largest value examined, is big enough to suggest that 2 is not a good asymptotic value for β at large N . The GOE value of $\beta = 1$ is still theoretically possible, but at the presently examined values of N we are still far from it, and the rate at which β decreases is already slowed down. A

⁶The distribution at $\beta = 0$ is close to but not the same as the Poisson distribution, for which $\langle r \rangle$ diverges while $\langle \tilde{r} \rangle \approx 0.386$.

⁷This is excepting the normalization, which becomes irrelevant once one takes the logarithmic derivative of the decay amplitude.

TABLE I. Dependence of $\langle r \rangle$ and β on N , based on samples of 2000 states at each N and J . The value of J is fixed to the value with a maximum number of partitions. The distributions are plotted in Fig. 2.

N	J	Total number of states	Points in sample	Per state	Average $\langle r_n \rangle$	Average $\langle \tilde{r}_n \rangle$	Fitted β
50	11	17,475	46,354	24	1.206	0.662	3.36
75	15	552,767	69,247	34	1.247	0.641	2.81
100	18	11.1×10^6	92,251	46	1.271	0.628	2.55
150	23	1.90×10^9	139,428	70	1.307	0.614	2.26
200	28	158×10^9	184,705	90	1.333	0.606	2.09
300	37	295×10^{12}	276,244	138	1.357	0.599	1.96
400	45	184×10^{15}	370,123	186	1.372	0.596	1.88
800	70	1.08×10^{26}	728,048	362	1.400	0.590	1.76
1600	109	4.22×10^{38}	1,446,008	720	1.413	0.588	1.72

TABLE II. Dependence of $\langle r \rangle$ and β on N , based on samples of 10,000 random partitions of N . The value of J is not fixed, but distributed as predicted by (4.20).

N	Total number of states	Points in sample	Per state	Average $\langle r_n \rangle$	Average $\langle \tilde{r}_n \rangle$	Fitted β
50	204,226	215,980	22	1.194	0.670	3.58
60	966,467	261,619	26	1.213	0.660	3.27
80	15.8×10^6	352,526	34	1.244	0.644	2.87
100	191×10^6	441,100	44	1.266	0.633	2.62
150	40.9×10^9	668,831	66	1.301	0.618	2.32
200	3.97×10^{12}	886,007	88	1.325	0.610	2.15

TABLE III. Dependence of $\langle r \rangle$ and β on J for $N = 100$. For each J we take 2000 states chosen at random. See plot in Fig. 3.

J	Total number of states	Points in sample	Per state	Average $\langle r_n \rangle$	Fitted β
6	143,247	155,162	80	1.203	3.60
10	2.98×10^6	126,008	64	1.241	2.95
14	8.86×10^6	105,502	54	1.263	2.65
18	11.1×10^6	92,251	46	1.271	2.55
22	9.24×10^6	83,405	42	1.276	2.52
26	6.32×10^6	76,211	38	1.272	2.57
30	3.91×10^6	70,650	30	1.262	2.69
50	204,226	51,287	26	1.209	3.38
70	5604	31,060	16	1.197	3.50

simple fit of the form $\beta(N) = a + b/N$ is in good agreement with all the values quoted in Table I and suggests $\beta = 1.68$ as the asymptotic value. On the other hand, a continuing logarithmic decrease cannot be ruled out from the data.

In addition, there is a dependence on J when N is fixed. In this case the average is greater for values of J for which there is a larger degeneracy. This is visible in Fig. 3, where we plot $\langle r_n \rangle$ alongside the logarithm of the number of partitions of length J at level $N = 100$. The plots do not match exactly, in particular the maximum points are at different values of J , but a correlation is visible. Then, the common observation from the dependence on N and J , is that the average appears to grow in correlation with the

number of degenerate states at the given level, but in a slow, at most logarithmic fashion.

VI. CHAOTIC FOUR-POINT SCATTERING PROCESS: ONE HES AND THREE TACHYONS

A. The scattering amplitude

The aim of this section is to analyze the chaotic behavior of the simplest four-point scattering amplitude involving one generic HES, i.e., scattering of three tachyons and one HES. In particular we will present the construction of the most general scattering amplitude based on the combination of the DDF formalism and string coherent state formalism, which is a suitable tool for the building of generating functions of amplitudes [19].

The cross symmetric generating scattering amplitude in Fig. 4 is composed of the following amplitudes⁸

$$\mathcal{A}_{\text{gen}}^{\text{HES}}(s, t, u) = \mathcal{A}_{\text{gen}}^{\text{HES}}(s, t) + \mathcal{A}_{\text{gen}}^{\text{HES}}(t, u) + \mathcal{A}_{\text{gen}}^{\text{HES}}(s, u), \quad (6.1)$$

where

$$\begin{aligned} \mathcal{A}_{\text{gen}}^{\text{HES}}(t, u) &= \mathcal{A}_{\text{gen}}^{\text{HES}}(s, t)|_{p_2 \leftrightarrow p_3}, \\ \mathcal{A}_{\text{gen}}^{\text{HES}}(s, u) &= \mathcal{A}_{\text{gen}}^{\text{HES}}(s, t)|_{p_1 \leftrightarrow p_2}. \end{aligned} \quad (6.2)$$

⁸We set $2\alpha' = 1$.

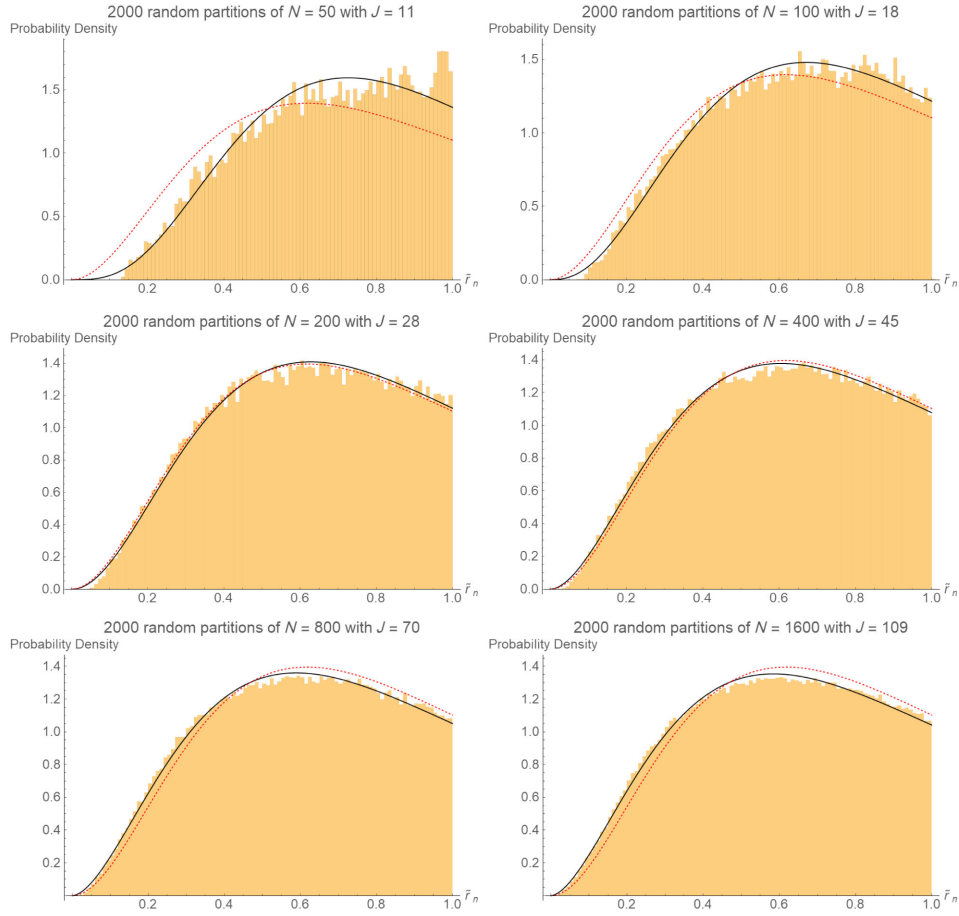


FIG. 2. The measured distributions of \tilde{r} across samples of 2000 states chosen at random with fixed N and J , fitted to a β -ensemble distribution (black line). The distribution is also compared to the GUE distribution (red, dashed). The fitting parameters are listed in Table I.

The generating amplitude of the process is given by

$$\mathcal{A}_{\text{gen}}^{\text{HES}}(s, t) = \int_0^1 dz z^{-\frac{s}{2}-2} (1-z)^{-\frac{t}{2}-2} \times e^{\sum_n \mathcal{J}_n \mathcal{O}_n(z) + \sum_{n,m} \mathcal{J}_n \mathcal{J}_m \mathcal{M}_{n,m}(z)}, \quad (6.3)$$

where the contribution proportional to the contractions $\zeta_n \cdot p_j$ is given by

$$\mathcal{O}_n(z) = \mathcal{T}_n^{(2)}(q \cdot p_3, q \cdot p_2; z) + \mathcal{T}_n^{(3)}(q \cdot p_3, q \cdot p_2; z) \quad (6.4)$$

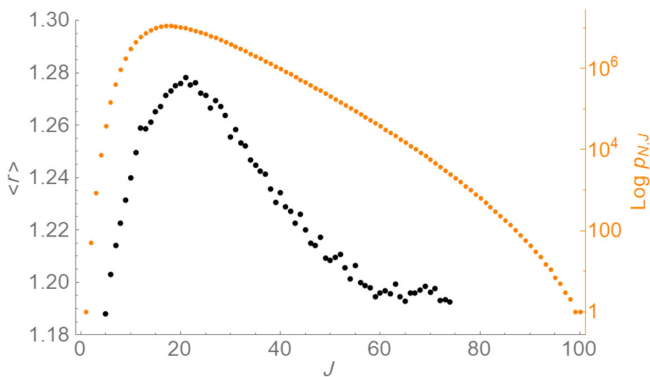


FIG. 3. The average value $\langle r_n \rangle$ as a function of J , where N is fixed at 100. The black dots are the measured values of $\langle r_n \rangle$ on samples of 2000 partitions at each helicity J . Also drawn is the number of states of a given J at $N = 100$, on a logarithmic scale. Some specific values are in Table III.

with the explicit form of the single contributions proportional to $\zeta_n \cdot p_2$ and $\zeta_n \cdot p_3$ (Appendix B)

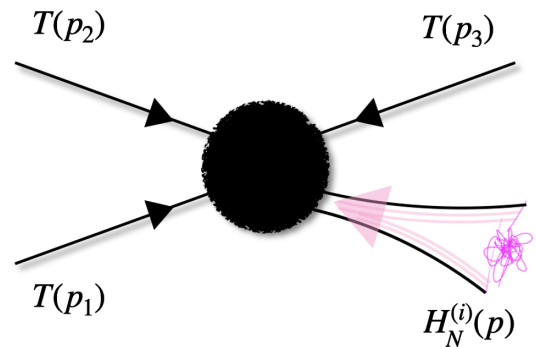


FIG. 4. Representative picture of the process under analysis.

$$\begin{aligned} \mathcal{T}_n^{(2)}(q \cdot p_3, q \cdot p_2; z) \\ = z \zeta_n \cdot p_2 \frac{(nq \cdot p_3)_{n-1}}{\Gamma(n)} {}_2F_1 \left(\begin{matrix} 1+nq \cdot p_2, 1-n \\ 2-n(1+q \cdot p_3) \end{matrix} \middle| z \right), \end{aligned} \quad (6.5)$$

$$\begin{aligned} \mathcal{T}_n^{(3)}(q \cdot p_3, q \cdot p_2; z) \\ = \zeta_n \cdot p_3 \frac{(1+nq \cdot p_3)_{n-1}}{\Gamma(n)} {}_2F_1 \left(\begin{matrix} nq \cdot p_2, 1-n \\ 1-n(1+q \cdot p_3) \end{matrix} \middle| z \right), \end{aligned} \quad (6.6)$$

while the contribution proportional to the contractions $\zeta_n \cdot \zeta_m$ can be written as

$$\begin{aligned} \mathcal{M}_{n,m}(z) = \zeta_n \cdot \zeta_m \sum_{k=1}^m k \frac{(nq \cdot p_3)_{n+k}}{(n+k)!} \\ \times {}_2F_1 \left(\begin{matrix} nq \cdot p_2, -n-k \\ 1-n(1+q \cdot p_3)-k \end{matrix} \middle| z \right) \frac{(mq \cdot p_3)_{m-k}}{(m-k)!} \\ \times {}_2F_1 \left(\begin{matrix} mq \cdot p_2, -m+k \\ 1-m(1+q \cdot p_3)+k \end{matrix} \middle| z \right). \end{aligned} \quad (6.7)$$

The projection of the amplitude onto a precise HES state insertion can be realized as follows:

$$\begin{aligned} \mathcal{A}(T(p_1), T(p_2), T(p_3), H_N(\{g_\ell\}; q, p)) \\ = \prod_{\ell=1}^N \left(\frac{d}{d\mathcal{J}_\ell} \right)^{g_\ell} \mathcal{A}_{\text{gen}}^{\text{HES}}(s, t) \Big|_{\{\mathcal{J}_n\}=0} \end{aligned} \quad (6.8)$$

since the identification between a precise HES state and the corresponding amplitude can be seen through the relation

$$\begin{aligned} \prod_{\ell=1}^N \frac{d^{g_\ell}}{d\mathcal{J}_\ell^{g_\ell}} e^{\sum_n \mathcal{J}_n \lambda_n \cdot A_{-n}} |\tilde{p}\rangle \Big|_{\{\mathcal{J}=0\}} = \prod_{\ell=1}^N (\lambda_\ell \cdot A_{-\ell})^{g_\ell} |\tilde{p}\rangle \\ = |\text{HES}, \{g_\ell\}\rangle_N, \end{aligned} \quad (6.9)$$

where \tilde{p} is the tachyonic reference momentum of the DDF formalism.

A compact representation of the generating scattering amplitude can be given by promoting the coefficients \mathcal{O}_n and $\mathcal{M}_{n,m}$ to derivative operators acting on a generating function of powers of z . In particular after the integration over z one has

$$\begin{aligned} \mathcal{A}_{\text{gen}}^{\text{HES}}(s, t) = \mathcal{A}_{\text{Ven}}(s, t) e^{\sum_n \mathcal{J}_n \mathcal{O}_n(\frac{d}{d\beta}) + \sum_{n,m} \mathcal{J}_n \mathcal{J}_m \mathcal{M}_{n,m}(\frac{d}{d\beta})} \\ \times {}_1F_1 \left(\begin{matrix} -\alpha' s - 1 \\ -\alpha' s - \alpha' t - 2 \end{matrix} \middle| \beta \right) \Big|_{\beta=0} \end{aligned} \quad (6.10)$$

this representation is a realization of the identification

$$\begin{aligned} \sum_{\ell} C_\ell \int_0^1 z^\ell z^{-\alpha' s - 2} (1-z)^{-\alpha' t - 2} \\ = \mathcal{B}(-\alpha' s - 1, -\alpha' t - 1) \sum_{\ell} C_\ell \frac{(-\alpha' s - 1)_\ell}{(-\alpha' s - \alpha' t - 2)_\ell}, \end{aligned} \quad (6.11)$$

where the coefficients C_ℓ are dictated by combinations of (6.4) and (6.7). We can observe a complete factorization between the partition structure and the pole structure, leading to a dressing factor of the Veneziano amplitude

$$\mathcal{A}_{\text{Ven}}(s, t) = \mathcal{B}(-\alpha' s - 1, -\alpha' t - 1). \quad (6.12)$$

B. The HES amplitude in the high-energy fixed-angle regime

In the kinematical regime where $s, |t| \gg 1$ and s/t is fixed, one can study the behavior the amplitude looking at the saddle point analysis of (6.3), where the saddle is located at $z^* = s/(s+t)$. Alternatively, one can obtain the same result studying (6.10) in the fixed angle limit where the action of the derivative operators turns out to be reproduced by the replacement $d/d\beta \rightarrow s/(s+t)$. The amplitude in fixed angle regime is then

$$\mathcal{A}_{\text{gen}}^{\text{HES}}(s, t) \Big|_{f.a} = \mathcal{A}_{\text{Ven}}^{f.a}(s, t) e^{\sum_n \mathcal{J}_n \mathcal{O}_n(\frac{s}{s+t}) + \sum_{n,m} \mathcal{J}_n \mathcal{J}_m \mathcal{M}_{n,m}(\frac{s}{s+t})}, \quad (6.13)$$

where the standard behavior of the Veneziano amplitude in this limit,

$$\mathcal{A}_{\text{Ven}}^{f.a}(s, t) \sim e^{-s \log s - t \log t + (s+t) \log(s+t)} \quad (6.14)$$

gets combined with an exponential dressing factor obtained by evaluating (6.5)–(6.7) at the saddle point $z^* = s/(s+t)$. To write the dressing factor more compactly, let us denote

$$\rho(s, \theta) \equiv -q \cdot p_2. \quad (6.15)$$

Following the kinematics (Appendix A), it always holds that $1+q \cdot p_3 = 2\rho$. Using this notation, the dressing factor will be made up of

$$\mathcal{T}_n^{(2)} \Big|_{z=z^*} = \frac{\zeta_n \cdot p_2}{\Gamma(n)} (2n\rho - n)_{n-1} z^* {}_2F_1 \left(\begin{matrix} 1-n\rho, 1-n \\ 2-2n\rho \end{matrix} \middle| z^* \right), \quad (6.16)$$

$$\mathcal{T}_n^{(3)} \Big|_{z=z^*} = \frac{\zeta_n \cdot p_3}{\Gamma(n)} (2n\rho - n + 1)_{n-1} {}_2F_1 \left(\begin{matrix} -n\rho, 1-n \\ 1-2n\rho \end{matrix} \middle| z^* \right), \quad (6.17)$$

and

$$\begin{aligned}
 \mathcal{M}_{n,m}|_{z=z^*} &= \zeta_n \cdot \zeta_m \sum_{k=1}^m k \frac{(-n-2n\rho)_{n+k}}{(n+k)!} {}_2F_1\left(\begin{matrix} -n\rho, -n-k \\ 1-2n\rho-k \end{matrix} \middle| z^* \right) \\
 &\times \frac{(-m-2m\rho)_{m-k}}{(m-k)!} {}_2F_1\left(\begin{matrix} -m\rho, -m+k \\ 1-2m\rho+k \end{matrix} \middle| z^* \right). \quad (6.18)
 \end{aligned}$$

The hypergeometric function ${}_2F_1(a, 1-n, c; z)$ for positive integer n is a polynomial in z of degree $n-1$. Using its explicit form one can rewrite the expressions as

$$\begin{aligned}
 \mathcal{T}_n^{(2)}|_{z=z^*} &= \frac{\zeta_n \cdot p_2}{\Gamma(n)} \sum_{k=0}^{n-1} \binom{n-1}{k} (2n\rho - n)_{n-k-1} \\
 &\times (1-n\rho)_k (z^*)^{k+1}, \quad (6.19)
 \end{aligned}$$

$$\begin{aligned}
 \mathcal{T}_n^{(3)}|_{z=z^*} &= \frac{\zeta_n \cdot p_3}{\Gamma(n)} \sum_{k=0}^{n-1} \binom{n-1}{k} (2n\rho - n + 1)_{n-k-1} \\
 &\times (-n\rho)_k (z^*)^k, \quad (6.20)
 \end{aligned}$$

from which one can see the dependence on the functions z^* and ρ is a polynomial one. One can also write the polynomial form of $\mathcal{M}_{n,m}$ in terms of a similar expansion.

To simplify the analysis of the amplitude, we can go to the specific case of identical circular polarizations, namely taking $\zeta_n = \zeta$ for all n , with $\zeta^2 = 0$.

In the case of circular polarizations, the terms $\mathcal{M}_{n,m}$ drop out and the amplitude in the fixed angle regime can be written as

$$\mathcal{A}_{f,a}^{\text{HES}} = \mathcal{A}_{\text{Ven}}^{f,a}(s, \theta) \prod_{n=1}^N (\mathcal{T}_n^{(2)}(s, \theta) + \mathcal{T}_n^{(3)}(s, \theta))^{g_n}. \quad (6.21)$$

From the kinematics in Appendix A, specialized to the high-energy, fixed angle regime one can use approximate forms for ρ , z^* , and $\zeta \cdot p_i$ when $s \gg 2N$, and reduce the expressions to

$$\begin{aligned}
 \mathcal{T}_n^{(2)}(s, \theta) &= \frac{z^*(\theta)\sqrt{s}}{2\Gamma(n)} (\rho(\theta) \cos \theta - 1) (2n\rho(\theta) - n)_{n-1} \\
 &\times {}_2F_1\left(\begin{matrix} 1-n\rho(\theta), 1-n \\ 2(1-n\rho(\theta)) \end{matrix} \middle| z^*(\theta) \right), \quad (6.22)
 \end{aligned}$$

$$\begin{aligned}
 \mathcal{T}_n^{(3)}(s, \theta) &= -\frac{\sqrt{s}}{\Gamma(n)} \rho(\theta) \cos \theta (2n\rho(\theta) - n + 1)_{n-1} \\
 &\times {}_2F_1\left(\begin{matrix} -n\rho(\theta), 1-n \\ 1-2n\rho(\theta) \end{matrix} \middle| z^*(\theta) \right), \quad (6.23)
 \end{aligned}$$

with

$$\rho(\theta) = \frac{1}{1 + \sin \theta}, \quad z^*(\theta) = \frac{1}{\cos^2(\theta/2)}. \quad (6.24)$$

The s dependence in the dressing factor reduces to a simple prefactor of $s^{J/2}$.

C. The HES amplitude in the Regge regime

In the kinematical regime where $s \gg |t|$ one can study the small angle dependence of the amplitude, in particular the amplitude behavior in the Regge regime is provided by (6.3) specialized around the leading contribution at $z = 1$. Alternatively it can be obtained from the representation (6.10) in the limit $s \gg t$. From the latter one can recover a trivial action of the derivative operators which corresponds to the replacement of $d/d\beta \rightarrow 1$. In any case the amplitude can be written as

$$\begin{aligned}
 \mathcal{A}_{\text{gen}}^{\text{HES}}(s, t)|_{\text{Regge}} &= \mathcal{A}_{\text{Ven}}^{\text{Regge}}(s, t) e^{\sum_n \mathcal{J}_n \mathcal{O}_n(1) + \sum_{n,m} \mathcal{J}_n \mathcal{J}_m \mathcal{M}_{n,m}(1)}, \quad (6.25)
 \end{aligned}$$

where there is the standard behavior of the Veneziano amplitude

$$\mathcal{A}_{\text{Ven}}^{\text{Regge}}(s, t) \sim \Gamma\left(-\frac{t}{2} - 1\right) s^{\frac{t}{2}+1} \quad (6.26)$$

and a nontrivial dressing factor made of the following contributions (see Appendix B for details):

$$\mathcal{O}_n(1) = (-)^n \zeta_n \cdot p_1 \frac{(1+nq \cdot p_1)_{n-1}}{\Gamma(n)}, \quad (6.27)$$

$$\mathcal{M}_{n,m}(1) = \zeta_n \cdot \zeta_m \frac{nm}{n+m} q \cdot p_1 (1+q \cdot p_1) \frac{\mathcal{O}_n(1)\mathcal{O}_m(1)}{\zeta_n \cdot p_1 \zeta_m \cdot p_1}. \quad (6.28)$$

Since $s \gg 2N$ and $s \gg |t|$ such that $\sin \theta \ll 1$, one can take simplified forms for the kinematic factors in appendix A, and see the explicit dependence on the angle. In particular one can take

$$q \cdot p_1 = -\frac{1}{1 + \sin \theta} \approx -1 + \sin \theta \quad (6.29)$$

to write

$$\mathcal{O}_n(1) \approx -\zeta_n \cdot p_1 \frac{\Gamma(n \sin \theta) \Gamma(n - n \sin \theta)}{\Gamma(n)} \sin(n\pi \sin \theta), \quad (6.30)$$

$$\mathcal{M}_{n,m}(1) \approx \zeta_n \cdot \zeta_m \frac{nm}{n+m} \sin \theta \frac{\mathcal{O}_n(1)\mathcal{O}_m(1)}{\zeta_n \cdot p_1 \zeta_m \cdot p_1}. \quad (6.31)$$

In the Regge regime, products of $\mathcal{M}_{n,m}(1)$ are suppressed since they contain higher powers of $\sin \theta$, allowing us to consider only the leading contributions provided by $\mathcal{O}_n(1)$.

The $\mathcal{M}_{n,m}$ can also be eliminated by a choice of circular polarizations.

Finally, we can write the Regge limit of the amplitude

$$\mathcal{A}_{\text{Regge}}^{\text{HES}} = \mathcal{A}_{\text{Ven}}^{\text{Regge}}(s, t) \prod_{n=1}^N (\mathcal{O}_n(1))^{g_n} \quad (6.32)$$

in an explicit form as

$$\begin{aligned} \mathcal{A}_{\text{Regge}}^{\text{HES}} &= \mathcal{A}_{\text{Ven}}^{\text{Regge}}(s, t) \left(-\sqrt{s} \left(1 - \frac{1}{2} \sin \theta \right) \right)^J \\ &\times \prod_{n=1}^N \left(\frac{\Gamma(n \sin \theta) \Gamma(n - n \sin \theta)}{\Gamma(n)} \sin(n\pi \sin \theta) \right)^{g_n}, \end{aligned} \quad (6.33)$$

where it was used that $\zeta \cdot p_1 \approx \sqrt{s}(1 - \frac{1}{2} \sin \theta)$ in this limit. The dressing factor of this amplitude bears strong resemblance to the three-point function of Eq. (5.1).

D. Spacing ratios for the four-point scattering amplitude

We will search for chaotic behavior in the scattering angle, by analyzing the ratios of spacings of consecutive peaks for the amplitude derived above. The procedure will be the same as the one described in Sec. VB 1.

We have seen that the amplitude can be factorized as the Veneziano amplitude times a dressing factor that depends on the HES state which we write as

$$\mathcal{A}_{\text{HES}}(s, t) = \mathcal{A}_{\text{Ven}}(s, t) \mathcal{D}_{\text{HES}}(s, \theta). \quad (6.34)$$

The dressing factor \mathcal{D}_{HES} is a complicated product of polynomials whose peaks are spaced erratically. We show that for solutions of

$$F_{\mathcal{D}}(\theta) \equiv \frac{d \log \mathcal{D}_{\text{HES}}}{d\theta} = 0 \quad (6.35)$$

the ratios of consecutive spacings will follow again the β -ensemble distribution, in both the fixed angle and Regge limits.

The interplay between the HES dressing factor and the Veneziano amplitude it multiplies can create a transition from chaotic to regular spacings, as will be discussed at the end of this section.

1. Chaotic behavior in the fixed angle regime

The dressing factor in the high energy limit was

$$\mathcal{D}_{\text{HES}}^{f.a.}(s, \theta) = \prod_{n=1}^N (\mathcal{T}_n^{(2)}(s, \theta) + \mathcal{T}_n^{(3)}(s, \theta))^{g_n}, \quad (6.36)$$

where we can write the polynomial form of $\mathcal{T}_n^{(2)}$ and $\mathcal{T}_n^{(3)}$ in this limit, which explicitly reads

$$\begin{aligned} \mathcal{T}_n^{(2)}(s, \theta) &= \frac{\sqrt{s}}{\Gamma(n)} (\rho(\theta) \cos \theta - 1) \sum_{k=0}^{n-1} \binom{n-1}{k} \\ &\times (2n\rho(\theta) - n)_{n-k-1} (1 - n\rho(\theta))_k \\ &\times \left(\frac{1}{\cos^2(\theta/2)} \right)^{k+1} \\ \mathcal{T}_n^{(3)}(s, \theta) &= \frac{\sqrt{s}}{\Gamma(n)} \rho(\theta) \cos \theta \sum_{k=0}^{n-1} \binom{n-1}{k} \\ &\times (2n\rho(\theta) - n + 1)_{n-k-1} (-n\rho(\theta))_k \\ &\times \left(\frac{1}{\cos^2(\theta/2)} \right)^k \end{aligned} \quad (6.37)$$

with $\rho(\theta) = 1/(1 + \sin \theta)$. Since the s dependence is only a prefactor in this limit it cannot affect the distribution of spacings.

Taking a sample of 2000 random partitions of $N = 100$, $J = 18$, we collect all the solutions of $d \log \mathcal{D}/d\theta = 0$ in the range $\theta \in (0, \frac{\pi}{2})$, and find the distribution plotted in Fig. 5. There are 29 data points per state in the sample.

We notice that there is an asymmetry in the distribution about $r \rightarrow 1/r$ with values $r > 1$ being favored, which causes it to deviate from the prediction. The average $\langle r_n \rangle$ is 1.497, while $\langle 1/r_n \rangle = 1.318$, where they should be equal. However, if one looks only at the normalized variable $\tilde{r} = \min(r, 1/r)$, which in a way symmetrizes the distribution, the agreement with the β -ensemble is improved considerably. It is not clear what is the reason that $r > 1$ is preferred, but the asymmetry could be a consequence of our looking solely at the part $\mathcal{A}(s, t)$ of the full amplitude, or of not looking at the full range of allowed angles.

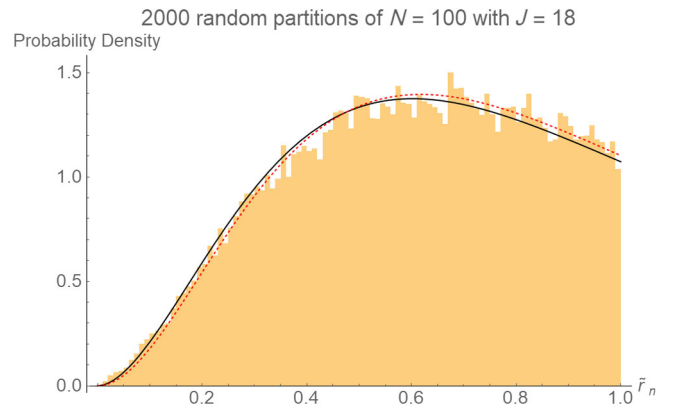


FIG. 5. Distribution for \tilde{r} for the dressing factor in the fixed angle limit. The best fit is with $\beta = 1.86$ (black line), which is very close to the GUE (dashed red line). The average value is $\langle \tilde{r}_n \rangle = 0.600$.

2. Chaotic behavior in the Regge regime

In the Regge regime, the dressing factor that depends on the HES state is

$$\mathcal{D}_{\text{HES}}^{\text{Regge}}(s, \theta) = \left(-\sqrt{s} \left(1 + \frac{\cos \theta}{1 + \sin \theta} \right) \right)^J \times \prod_n \left(\frac{(1 - n + \frac{n}{1 + \sin \theta})_{n-1}}{\Gamma(n)} \right)^{g_n}, \quad (6.38)$$

where in the present analysis we take Eq. (6.32) before the small angle approximation. This is done mainly for practical reasons, since we have to go beyond small angles ($\sin \theta \ll 1$) to collect enough data points for the statistical analysis.⁹

It has almost the same form as the three-point amplitude of Eq. (5.1) after the replacement of $\cos^2 \frac{\theta}{2} \rightarrow 1/(1 + \sin \theta)$. Each term in the product is a polynomial in $1/(1 + \sin \theta)$. The dependence of the dressing factor on s is trivial, and the logarithmic derivative of the dressing factor is a function only of θ of a simple enough form

$$F_{\mathcal{D}}(\theta) = \frac{d \log \mathcal{D}_{\text{HES}}^{\text{Regge}}}{d\theta} = -\frac{J}{1 + \cos \theta + \sin \theta} - \frac{\cos \theta}{1 + \sin \theta} \sum_{n=1}^N g_n \sum_{k=1}^{n-1} \frac{n}{n - k(1 + \sin \theta)}. \quad (6.39)$$

We can find the zeros of this function of θ and plot the distribution of \tilde{r}_n for their spacings, when considering only zeros in the range $\theta \in (0, \frac{\pi}{4})$. The results are similar to what we obtained in the fixed-angle regime in the previous subsection, with a slightly skewed distribution that agrees well with the β -ensemble distribution once we symmetrize it. See Fig. 6.

3. Transition from chaotic to regular behavior

The interplay between the Veneziano amplitude and its dressing factor can create a transition from chaotic to regular spacings as one moves from small to large angles.

The erratic dressing factor is multiplied by the Veneziano amplitude, which is a highly oscillatory function of the angle at high energies, but one that is regular in the sense that it has regularly spaced zeros as a function of t , which leads to almost regularly spaced peaks of the amplitude between these zeros. As a function of θ these zeros become denser at large angles, but remain quite regular. In the interplay between the Veneziano and the HES dressing factors, the spacings between peaks depend on which of the

⁹An alternative would be to use (6.33) and ignore the fact that we assumed $\sin \theta \ll 1$ to get it. That dressing factor will also have a similar distribution of r_n .

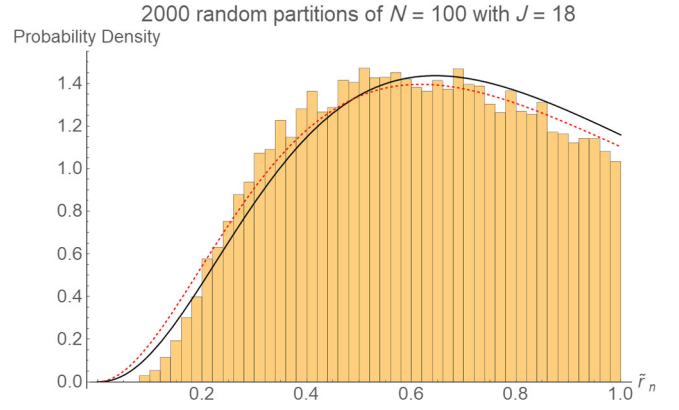


FIG. 6. Distribution for \tilde{r} for the dressing factor in the Regge limit. We take zeros in the range $\theta \in (0, \pi/4)$ and find 17 points per state. The average of $\langle \tilde{r}_n \rangle$ is 0.605 and the best fit (black) has $\beta = 2.27$. The distribution is also close to GUE (red, dashed).

two is oscillating faster. For large angles, the Veneziano factor will usually dominate and cause the peaks to be regularly spaced, while at smaller angles one can see the chaotic spacings coming from the HES factor.

Whether we can see these two regimes clearly will depend on the scattering energy, and on the level of the HES state. It is somewhat difficult to find the range of parameters (s and N) where this can be computed and seen clearly. One example in which we see it in the Regge limit amplitude of (6.33).¹⁰

Recall that the full form of the Veneziano amplitude in the Regge limit is

$$\mathcal{A}_{\text{Ven}}^{\text{Regge}}(s, t) = \frac{\sin[\pi\alpha'(s+t)]}{\sin(\pi\alpha's)} \Gamma(-\alpha't - 1) (\alpha's)^{\alpha't+1}. \quad (6.40)$$

Importantly, here we retain the oscillating factor which is usually averaged over in discussing the Regge behavior. Taking the log derivative we get the term

$$\frac{d \log \mathcal{A}_{\text{Ven}}^{\text{Regge}}}{d\theta} = \frac{dt}{d\theta} \alpha' (\log(\alpha's) + \pi \cot[\pi\alpha'(s+t)] - \psi(-\alpha't - 1)) \quad (6.41)$$

which is a complicated function of the angle with many zeros, which are almost regularly spaced. Note the implicit dependence on the level N which enters through the kinematic relation of $t(\theta)$.

Now, in studying the distribution of zeros of the log-derivative of the full amplitude,

¹⁰This is not an optimal example, since we should not trust (6.33) away from small angles. We choose it for illustration purposes, and because it is the simplest amplitude that we can write that realizes this transition in an explicit and easy to calculate way.

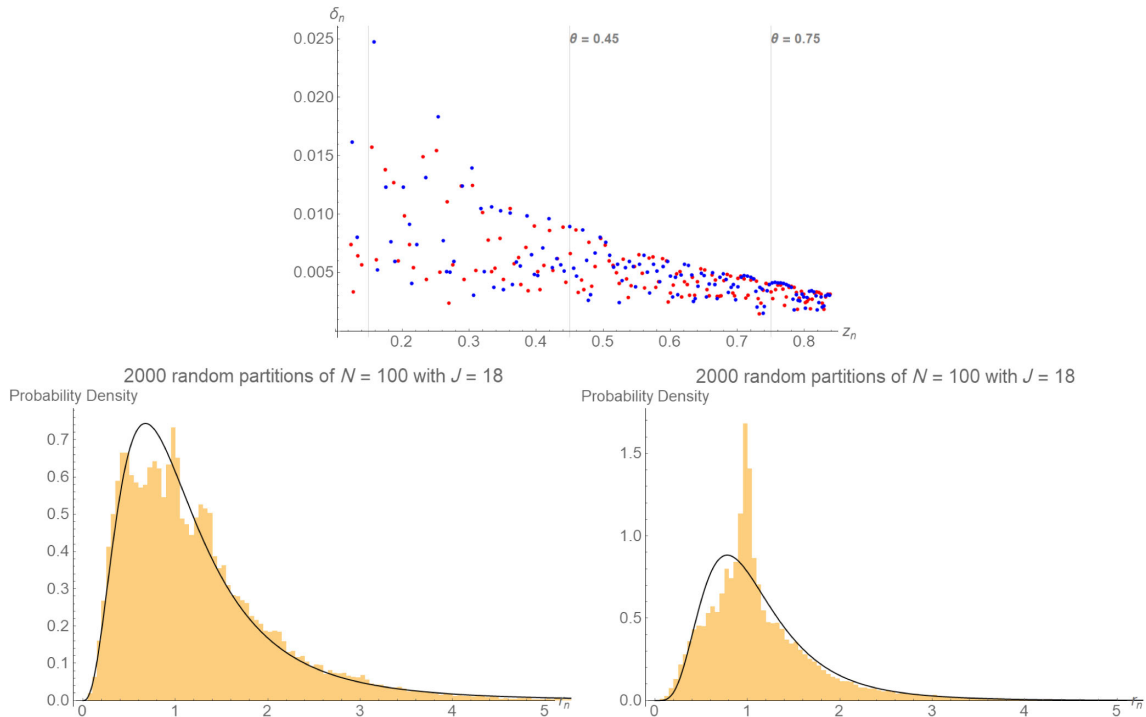


FIG. 7. Top: The spacings δ_n as a function of z_n for two random states of $N = 100$. The spacings exhibit a transition from random to regular behavior. Bottom: The distribution of spacing ratios (r_n) for zeros in the ranges $\theta \in (0.15, 0.45)$ (left) and $\theta \in (0.15, 0.75)$ (right). In the latter, a narrow peak around $r = 1$ appears on top of the chaotic distribution.

$$F(\theta) = \frac{d \log \mathcal{A}_{\text{Ven}}^{\text{Regge}}}{d\theta} + \frac{d \log \mathcal{D}_{\text{HES}}^{\text{Regge}}}{d\theta} = 0 \quad (6.42)$$

we can observe a transition between the chaotic and regular spacings, as illustrated in Fig. 7.

VII. SUMMARY AND OUTLOOK

We have expanded on the analysis of string scattering amplitudes involving an HES state, randomly chosen among the huge number of states with the given mass ($\alpha' M^2 = N - 1 = \sum_n n g_n - 1$) and helicity J ($N = S_{\text{Max}} \geq S \geq J = \sum_n g_n$). In [4] we fitted the spacing ratios to a log-normal distribution. Although the log-normal distribution proved to be a good approximation of the available results, in the present work we have improved and argued that the β -ensemble distribution represents a better fit for the larger and finer set of data analyzed here. Moreover we have also argued that the β -ensemble distribution is better motivated by physical considerations.

We observed the chaotic behavior in the angular dependence of scattering amplitudes involving one highly excited string state. We can ascribe the chaos to the random superposition of the relevant spherical harmonics in the partial wave expansion of the amplitude. Given the unitarity of the process (the overall normalization is irrelevant in the analysis) we would expect β -ensemble distribution with $\beta = 2$ as for GUE, or equivalently for large N , CUE. Instead we found better fits with values of β around 1.7; not

far from 2 but significantly different from it such that the distribution cannot be precisely that of GUE. Comparing our data to similar samples drawn directly from GUE can confirm that deviations from $\beta = 2$ are expected, but they are smaller than what we observed.

The scattering amplitude of HES states and three tachyons which we derived and analyzed in various regimes shows chaotic behavior associated to a dressing factor multiplying the ‘standard’ Veneziano amplitude. In this case we did not examine in as much detail the dependences of the distributions on N and J , but our observation is that the general behavior is the same as in the three-point function.

There are several possible directions for followup work:

- (i) One should try and clarify the origin of the mild but non-negligible dependence of the fitted β parameter and the average ratio $\langle r \rangle$ on the chosen data, most prominently on N and J .
- (ii) One could conceive extending the analysis to processes with two or more HES states. The first obvious choice that comes to mind is generalized Compton scattering of a low-mass probe off HES states, possibly including inelastic channels involving excitations of the HES itself (to a nearby HES state). A related amplitude was computed already in [36].
- (iii) One could consider similar processes in hadronic models inspired by holographic QCD, along the lines of [37,38] and prove or disprove the emergence of chaotic behavior in this context.

- (iv) Finding other tractable examples for chaos in quantum scattering amplitudes is another important task. In [4] we have discussed the leaky torus as another example where an analytic formula is known [6]. Another example of chaotic quantum scattering is in [39].
- (v) One could give further quantitative support to the string/black hole correspondence by relating the “measurable” chaotic behavior found here with the expected chaotic behavior of scattering, absorption, and thermalization in black hole processes [40–51]. To this end, a given HES state, that may be considered a (a)typical microstate of a putative black hole ensemble, would better be replaced with a coherent state with mass, charge and spin distributed around some large “classical” value. Using the results in [19] could prove crucial in this endeavor.
- (vi) In [3], it was observed that while the spectra of some nonintegrable QFT models displayed chaotic behavior, the associated distribution of eigenvectors did not match the RMT expectations, and was in fact unchanged from the integrable, nonchaotic models. One should identify what are the eigenvectors associated with the scattering amplitudes and verify if they are distributed as predicted by RMT. This has consequences for thermalization, as stressed in [3]. We hope to report soon on some of the above issues.

ACKNOWLEDGMENTS

We would like to thank R. Benzi, B. Craps, K. Hashimoto, G. Parisi, G. Salina, F. Popov, D. Gross, S. Negro, V. Rosenhaus, S. Yankielowicz, P. Di Vecchia, B. Sundborg, E. Kiritsis, V. Niarchos and T. Yoda for useful discussions. The work of M. B. and M. F. is partially supported by the MIUR PRIN Grant No. 2020KR4KN2 “String Theory as a bridge between Gauge Theories and Quantum Gravity”. The work of J. S. was supported by a center of excellence of the Israel Science Foundation (Grant No. 2289/18). D. W. was supported by an appointment to the YST Program at the APCTP through the Science and Technology Promotion Fund and Lottery Fund of the Korean Government. This was also supported by the Korean Local Governments—Gyeongsangbuk-do Province and Pohang City. In the early stages of this project D. W. was supported by the Quantum Gravity Unit of the Okinawa Institute of Science and Technology Graduate University (OIST).

APPENDIX A: FOUR-POINT AMPLITUDE KINEMATICS

Let us introduce the center-of-mass (c.m.) system kinematics of scattering three tachyons of momenta p_1 , p_2 , and p_3 with an HES state of momentum p .

We choose the momenta of the scattered states as

$$p_1 = (E_1, p_{\text{in}}, 0, \vec{0}), \quad p_2 = (E_2, -p_{\text{in}}, 0, \vec{0}) \quad (\text{A1})$$

$$p_3 = -(E_3, p_{\text{out}} \cos \theta, p_{\text{out}} \sin \theta, \vec{0}),$$

$$p = -(E_4, -p_{\text{out}} \cos \theta, -p_{\text{out}} \sin \theta, \vec{0}) \quad (\text{A2})$$

such that

$$p_1 + p_2 = \sqrt{s}, \quad p_1 + p_2 + p_3 + p = 0. \quad (\text{A3})$$

The DDF reference lightlike momentum q and polarization λ are constrained by $q \cdot p = 1^{11}$ and $\lambda \cdot q = 0$, and they are represented by

$$q = \frac{(1, 0, 1, \vec{0})}{E_4 + \sin \theta p_{\text{out}}}, \quad \lambda = \frac{(0, 1, 0, \vec{\Lambda})}{\sqrt{1 + \vec{\Lambda} \cdot \vec{\Lambda}^*}}. \quad (\text{A4})$$

Since, for simplicity, we chose to work with “null” λ , $\lambda \cdot \lambda = 0$, we may choose a complex $\vec{\Lambda}$ such that $\vec{\Lambda} \cdot \vec{\Lambda} = -1$ and yet $\vec{\Lambda} \cdot \vec{\Lambda}^* = +1$.

Following the CMS kinematics one has

$$E_1 = \frac{s + M_1^2 - M_2^2}{2\sqrt{s}} = \frac{\sqrt{s}}{2},$$

$$E_2 = \frac{s + M_2^2 - M_1^2}{2\sqrt{s}} = \frac{\sqrt{s}}{2}, \quad (\text{A5})$$

$$E_3 = \frac{s + M_3^2 - M_4^2}{2\sqrt{s}} = \frac{s - 2N}{2\sqrt{s}},$$

$$E_4 = \frac{s + M_4^2 - M_3^2}{2\sqrt{s}} = \frac{s + 2N}{2\sqrt{s}}, \quad (\text{A6})$$

and

$$p_{\text{in}}^2 = 2 + \frac{s}{4}; \quad p_{\text{out}}^2 = 2 + \frac{s}{4} \left(1 - \frac{2N}{s}\right)^2. \quad (\text{A7})$$

The relevant scalar products involving momenta are given by

$$q \cdot p_1 = -\frac{E_1}{\sin \theta p_{\text{out}} + E_4}$$

$$= \frac{-1}{1 + \frac{2N}{s} + 2 \sin \theta \sqrt{\frac{2}{s} + \frac{1}{4} \left(1 - \frac{2N}{s}\right)^2}} = q \cdot p_2, \quad (\text{A8})$$

$$q \cdot p_3 = \frac{E_3 - p_{\text{out}} \sin \theta}{E_4 + p_{\text{out}} \sin \theta} = \frac{1 - \frac{2N}{s} - 2 \sin \theta \sqrt{\frac{2}{s} + \frac{1}{4} \left(1 - \frac{2N}{s}\right)^2}}{1 + \frac{2N}{s} + 2 \sin \theta \sqrt{\frac{2}{s} + \frac{1}{4} \left(1 - \frac{2N}{s}\right)^2}}. \quad (\text{A9})$$

¹¹Here and throughout we work in units where $\alpha' = \frac{1}{2}$.

Using conservation of momentum and $q \cdot p = 1$ one can easily derive the relation

$$q \cdot p_3 = -1 - q \cdot (p_1 + p_2) = -1 - 2q \cdot p_1. \quad (\text{A10})$$

The relevant scalar products involving polarizations are given by

$$\lambda \cdot p = p_{\text{out}} \cos \theta = \sqrt{s} \cos \theta \sqrt{\frac{2}{s} + \frac{1}{4} \left(1 - \frac{2N}{s}\right)^2} = -\lambda \cdot p_3, \quad (\text{A11})$$

$$\lambda \cdot p_1 = p_{\text{in}} = \sqrt{s} \sqrt{\frac{2}{s} + \frac{1}{4}} = -\lambda \cdot p_2, \quad (\text{A12})$$

where for convenience it was constrained the free parameter to be $\vec{\Lambda} \cdot \vec{\Lambda} = -1$. Given the general form of the covariant polarization $\zeta^\mu = \lambda^\mu - \lambda \cdot p q^\mu$, it follows that

$$\zeta \cdot p_1 = \sqrt{s} \sqrt{\frac{2}{s} + \frac{1}{4}} + \frac{\sqrt{s} \cos \theta \sqrt{\frac{2}{s} + \frac{1}{4} \left(1 - \frac{2N}{s}\right)^2}}{1 + \frac{2N}{s} + 2 \sin \theta \sqrt{\frac{2}{s} + \frac{1}{4} \left(1 - \frac{2N}{s}\right)^2}}, \quad (\text{A13})$$

$$\zeta \cdot p_2 = -\sqrt{s} \sqrt{\frac{2}{s} + \frac{1}{4}} + \frac{\sqrt{s} \cos \theta \sqrt{\frac{2}{s} + \frac{1}{4} \left(1 - \frac{2N}{s}\right)^2}}{1 + \frac{2N}{s} + 2 \sin \theta \sqrt{\frac{2}{s} + \frac{1}{4} \left(1 - \frac{2N}{s}\right)^2}}, \quad (\text{A14})$$

$$\zeta \cdot p_3 = -\frac{2\sqrt{s} \cos \theta \sqrt{\frac{2}{s} + \frac{1}{4} \left(1 - \frac{2N}{s}\right)^2}}{1 + \frac{2N}{s} + 2 \sin \theta \sqrt{\frac{2}{s} + \frac{1}{4} \left(1 - \frac{2N}{s}\right)^2}}, \quad (\text{A15})$$

where the combination of these terms reflects momentum conservation $\zeta \cdot (p_1 + p_2 + p_3) = 0$ and transversality $\zeta \cdot p = 0$, as expected.

APPENDIX B: DERIVATION OF THE HES-THREE TACHYON AMPLITUDE

In this section we will review the main steps for the computation of the scattering amplitude involving three tachyons and one generic HES state in an open bosonic string. Let us start by considering the tachyonic vertex operators inserted in the ordered positions z_j of the disk, with $j = 1, 2, 3$

$$V_T(p_j, z_j) = e^{ip_j \cdot X(z_j)} \quad (\text{B1})$$

and the coherent vertex operator inserted in position z_4 ,

$$V_C(p, z_4) = \exp\left(\sum_{n,m} \frac{\zeta_n \cdot \zeta_m}{2} \mathcal{S}_{n,m} e^{-i(n+m)q \cdot X} + \sum_n \zeta_n \cdot \mathcal{P}_n e^{-inq \cdot X} + i\tilde{p} \cdot X\right)(z_4). \quad (\text{B2})$$

The generating scattering amplitude is given by

$$\mathcal{A}_{\text{gen}}^{\text{HES}}(s, t) = \int_{z_4}^{z_2} \prod_{\ell=1}^4 dz_\ell \langle V_T(p_1, z_1) V_T(p_2, z_2) \times V_T(p_3, z_3) V_C(p, z_4) \rangle. \quad (\text{B3})$$

From the correlator one can factorize the Koba-Nielsen contribution due to the contractions

$$\langle p_j \cdot X(z_j) p_\ell \cdot X(z_\ell) \rangle = -p_j \cdot p_\ell \log(z_{j\ell}), \quad (\text{B4})$$

$$z_{j\ell} = z_j - z_\ell$$

finding

$$KN(\{z_j\}) = z_{12}^{p_1 \cdot p_2} z_{13}^{p_1 \cdot p_3} z_{14}^{p_1 \cdot p} z_{23}^{p_2 \cdot p_3} z_{24}^{p_2 \cdot p} z_{34}^{p_3 \cdot p}. \quad (\text{B5})$$

Using the general kinematics

$$\begin{aligned} (p_3 + p)^2 &= -s = (p_1 + p_2)^2, \\ (p_2 + p_3)^2 &= -t = (p_1 + p)^2, \\ (p_1 + p_3)^2 &= -u = (p_2 + p)^2, \end{aligned} \quad (\text{B6})$$

where $s + t + u = 3M_T^2 + M_N^2$ with $M_N^2 = 2(N-1)$ the mass square of a generic state of the level N , the Koba-Nielsen contribution can be written as

$$KN(\{z_j\}) = \left(\frac{z_{12}z_{34}}{z_{13}z_{24}}\right)^{-\frac{1}{2}-2} \left(\frac{z_{14}z_{23}}{z_{13}z_{24}}\right)^{-\frac{1}{2}-2} \times (z_{13}z_{24})^{-2} \left(\frac{z_{34}z_{14}}{z_{13}}\right)^N. \quad (\text{B7})$$

The last factor is related to the exponential nature of the insertion (B2), and it can be reabsorbed as a dressing factor of the linear and bilinear contributions

$$e^{-inq \cdot X} \Rightarrow \left(\frac{z_{34}z_{14}}{z_{13}}\right)^n, \quad e^{-i(m+n)q \cdot X} \Rightarrow \left(\frac{z_{34}z_{14}}{z_{13}}\right)^{m+n}. \quad (\text{B8})$$

The remaining contributions are related to the contractions

$$\langle p_j \cdot X(z_j) \zeta_n \cdot \partial X(z_4) \rangle = \frac{\zeta_n \cdot p_j}{z_{j4}} \quad (\text{B9})$$

that combined with the operator structure $\zeta_n \cdot \mathcal{P}_n$ and $\mathcal{S}_{n,m}$ yield

$$\zeta_n \cdot \mathcal{P}_n(z_4) \Rightarrow \sum_{k=1}^n \left(\prod_{j \neq 4} \frac{\zeta_n \cdot p_j}{z_{j4}} \right) \mathcal{Z}_{n-k} \left(n \sum_{j \neq 4} \frac{q \cdot p_j}{z_{j4}} \right) \quad (\text{B10})$$

and

$$S_{n,m}(z_4) = \sum_{r=1}^m r \mathcal{Z}_{n+r} \left(n \sum_{j \neq 4} \frac{q \cdot P_j}{z_{j4}} \right) \mathcal{Z}_{m-r} \left(m \sum_{j \neq 4} \frac{q \cdot P_j}{z_{j4}} \right). \quad (\text{B11})$$

The combination of all the contractions yields

$$\begin{aligned} \mathcal{A}_{\text{gen}}^{\text{HES}}(s, t) &= \int_{z_4}^{z_2} \prod_{\ell=1}^4 dz_{\ell} \left(\frac{z_{12}z_{34}}{z_{13}z_{24}} \right)^{-\frac{s}{2}-2} \left(\frac{z_{14}z_{23}}{z_{13}z_{24}} \right)^{-\frac{t}{2}-2} (z_{13}z_{24})^{-2} \\ &\times \exp \left\{ \sum_n \left(\frac{z_{34}z_{14}}{z_{13}} \right)^n \sum_{k=1}^n \left(\prod_{j \neq 4} \frac{\zeta_n \cdot P_j}{z_{j4}} \right) \mathcal{Z}_{n-k} \left(n \sum_{j \neq 4} \frac{q \cdot P_j}{z_{j4}} \right) \right\} \\ &\times \exp \left\{ \sum_{n,m} \frac{\zeta_n \cdot \zeta_m}{2} \left(\frac{z_{34}z_{14}}{z_{13}} \right)^{n+m} \sum_{r=1}^m r \mathcal{Z}_{n+r} \left(n \sum_{j \neq 4} \frac{q \cdot P_j}{z_{j4}} \right) \mathcal{Z}_{m-r} \left(m \sum_{j \neq 4} \frac{q \cdot P_j}{z_{j4}} \right) \right\}. \end{aligned} \quad (\text{B12})$$

Eliminating the redundancy of the $SL(2, R)$ invariance fixing z_1, z_2 , and z_4 produces the standard transformation of the integration measure

$$\prod_{j=1}^4 dz_j = z_{12}z_{14}z_{24} dz_3 \quad (\text{B13})$$

which combined with $(z_{13}z_{24})^{-2}$ gives a finite result in the limit $z_1 = \infty, z_2 = 1, z_3 = z, z_4 = 0$

$$\frac{z_{12}z_{14}}{z_{13}^2 z_{24}} \Big|_{z_1=\infty} = 1, \quad (\text{B14})$$

while for the other terms one has

$$\left(\frac{z_{12}z_{34}}{z_{13}z_{24}} \right)^{-\frac{s}{2}-2} = z^{-\frac{s}{2}-2}, \quad \left(\frac{z_{14}z_{23}}{z_{13}z_{24}} \right)^{-\frac{t}{2}-2} = (1-z)^{-\frac{t}{2}-2}. \quad (\text{B15})$$

Finally, one can study how the remaining contributions transform under the $SL(2, R)$ invariance, finding the final expression of the scattering amplitude given in (6.3).

APPENDIX C: COMPARISON OF THE β -ENSEMBLE WITH A LOG-NORMAL DISTRIBUTION

In our previous paper [4] we fitted the spacing ratios r_n to a log-normal distribution

$$f_{\text{LN}}(r) = \frac{1}{\sqrt{2\pi\sigma^2}r} \exp \left(-\frac{[\log(r) - \mu]^2}{2\sigma^2} \right). \quad (\text{C1})$$

This distribution proved good as a first approximation of the result, but in the present work we have seen that the β -ensemble distribution (3.4) is both a better fit for the data, and is better motivated by random matrix theory.

The distributions are quite close. For a given β we can find a log-normal distribution with $\mu = 0$ (because of the $r \rightarrow 1/r$ symmetry) and an appropriate value of σ to approximate it very well. One can measure the distance between the distributions using the relative entropy,

$$I(\beta; \sigma) = \int_0^\infty dr f_{\beta}(r) \log \left(\frac{f_{\beta}(r)}{f_{\text{LN}}(r)} \right) \quad (\text{C2})$$

and, for a given β , pick the value of σ that minimizes it. For instance, for $\beta = 1, 2$, and 4 the closest log-normal distributions are at $\sigma \approx 1.014, 0.773$, and 0.565 , respectively. The value of the relative entropy at the minimum is in these three cases between 0.002 – 0.009 , with the better agreement occurring for larger β .

For a direct comparison, in Fig. 8 we plot one of the distribution we had in Sec. V, for the decay amplitude of states with $N = 400$, now together with a fitted log-normal

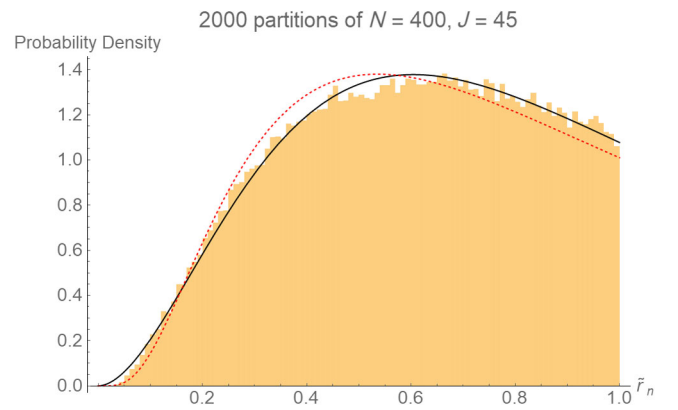


FIG. 8. Distribution of spacing ratios in the decay amplitude of states with $N = 400$, fitted to a log-normal distribution with $\sigma = 0.79$ (dashed-red line) and to the β -ensemble (black line) distribution with $\beta = 1.88$. The better fit is with β .

distribution. We would also note that in [4] we used an approximated form of the HES $\rightarrow TT$ amplitude (5.1) which separately caused deviations in the result for the spacing ratios. The excess of points around $r = 1$ noted there does not occur when we use the exact formula.

APPENDIX D: RANDOM PARTITIONS OF A LARGE INTEGER

As discussed in Sec. IV B, the number of partitions of an integer N grows exponentially in \sqrt{N} . Since we cannot probe the full space of states, we need a reliable method of picking representative, generic states in a random way.

Picking a partition of a large integer N at random, with each partition having an equal probability of being chosen, is a nontrivial task. We present here one algorithm that accomplishes this goal.

We represent a partition as a list $\{g_n\}$, $n = 1, 2, \dots, N$, where g_n is the number of times that n occurs in the partition. The algorithm relies on a result [52] regarding the asymptotic distributions of $\{g_n\}$ for large N , namely that each g_n has the geometric distribution

$$P(g_n = k) = (1 - p_n)^k p_n \quad (\text{D1})$$

with the parameter

$$p_n = 1 - \exp\left(-\frac{n\pi}{\sqrt{6N}}\right). \quad (\text{D2})$$

One can generate a random partition of N by drawing values of $\{g_n\}$, $n = 1, 2, \dots, N$ from the above distribution, treating each g_n as an independent variable, until one reaches a set that corresponds to a partition of N . That is, until one gets a set of $\{g_n\}$ that satisfies $\sum_n n g_n = N$. The result of [52] implies that the partitions of N that will be reached by this algorithm will be uniformly distributed, at

least at large N . Each partition of N has an equal probability of being chosen.

The downside of the algorithm is that it needs to reject many sets of $\{g_n\}$ until it reaches one that satisfies the constraint, with the expected number of rejections being $\mathcal{O}(N^{3/4})$. By use of probabilistic algorithms one can improve the number of rejections to $\mathcal{O}(N^{1/4})$ or even $\mathcal{O}(1)$ [53].

The simpler, $\mathcal{O}(N^{1/4})$ algorithm is as follows:

- (1) Draw $\{g_n\}$ for $n \geq 2$, with g_n distributed according to (D1).
- (2) Set $k \equiv N - \sum_{n=2}^N n g_n$. If $k < 0$, restart from step 1.
- (3) Draw a random variable $u \in (0, 1)$ from the uniform continuous distribution. If $u < e^{-\frac{ku}{\sqrt{6N}}}$, reject the partition and return to step 1.
- (4) Else, set $g_1 = k$ to finish.

Step 3, where some partitions are rejected with a specifically chosen probability, assures that the probability to output any given partition is as before.

We can use a modification of the above algorithm to generate a partition of a given length J . We modify only step 1, where we start by choosing $\{g_n\}$ such that $g_J \geq 1$ and $g_{n>J} = 0$. Then, the result after step 4 will be a partition of N where the maximum summand in the partition is $n_{\max} = J$. Then, taking the conjugate partition, we get a partition of N into exactly J parts.

In the preparation of this work, we have used several methods of picking random partitions. One is the brute force method; generate a list of all possible partitions of a given N (and J when that is constrained), then, select random elements from the list with equal probability. This is the simplest method at smaller N , but becomes impractical quickly as one increases N . For unconstrained partitions of N we have used Mathematica's built-in (as part of the Combinatorica package) function `RandomPartition[N]`. To produce partitions of large N with fixed J , we have used the algorithm described in the previous paragraph.

-
- [1] M. Mehta, *Random Matrices*, 3rd ed. (Elsevier Science, New York, 2004), [10.1016/S0079-8169\(04\)80091-6](https://doi.org/10.1016/S0079-8169(04)80091-6).
 - [2] G. Akemann, J. Baik, and P. Di Francesco, *The Oxford Handbook of Random Matrix Theory* (Oxford University Press, New York, 2015), [10.1093/oxfordhb/9780198744191.001.0001](https://doi.org/10.1093/oxfordhb/9780198744191.001.0001).
 - [3] M. Srdinšek, T. Prosen, and S. Sotiriadis, Signatures of Chaos in Nonintegrable Models of Quantum Field Theories, *Phys. Rev. Lett.* **126**, 121602 (2021).
 - [4] M. Bianchi, M. Firrotta, J. Sonnenschein, and D. Weissman, Measure for Chaotic Scattering Amplitudes, *Phys. Rev. Lett.* **129**, 261601 (2022).
 - [5] V. Rosenhaus, Chaos in the Quantum Field Theory S-Matrix, *Phys. Rev. Lett.* **127**, 021601 (2021).
 - [6] M. C. Gutzwiller, Stochastic behavior in quantum scattering, *Physica (Amsterdam)* **7D**, 341 (1983).
 - [7] M. V. Berry, Riemann's zeta function: A model for quantum chaos?, in *Quantum Chaos and Statistical Nuclear Physics*, edited by T. H. Seligman and H. Nishioka (Springer, Berlin, Heidelberg, 1986), pp. 1–17.
 - [8] A. M. Odlyzko, On the distribution of spacings between zeros of the zeta function, *Math. Comput.* **48**, 273 (1987).
 - [9] D. J. Gross and V. Rosenhaus, Chaotic scattering of highly excited strings, *J. High Energy Phys.* **05** (2021) 048.
 - [10] V. Rosenhaus, Chaos in a Many-String Scattering Amplitude, *Phys. Rev. Lett.* **129**, 031601 (2022).
 - [11] G. T. Horowitz and J. Polchinski, A correspondence principle for black holes and strings, *Phys. Rev. D* **55**, 6189 (1997).

- [12] T. Damour and G. Veneziano, Selfgravitating fundamental strings and black holes, *Nucl. Phys.* **B568**, 93 (2000).
- [13] M. V. Berry and M. Tabor, Level clustering in the regular spectrum, *Proc. R. Soc. A* **356**, 375 (1977).
- [14] O. Bohigas, M. J. Giannoni, and C. Schmit, Characterization of Chaotic Quantum Spectra and Universality of Level Fluctuation Laws, *Phys. Rev. Lett.* **52**, 1 (1984).
- [15] V. Oganesyan and D. A. Huse, Localization of interacting fermions at high temperature, *Phys. Rev. B* **75**, 155111 (2007).
- [16] E. Del Giudice, P. Di Vecchia, and S. Fubini, General properties of the dual resonance model, *Ann. Phys. (N.Y.)* **70**, 378 (1972).
- [17] M. Hindmarsh and D. Skliros, Covariant Closed String Coherent States, *Phys. Rev. Lett.* **106**, 081602 (2011).
- [18] D. Skliros and M. Hindmarsh, String vertex operators and cosmic strings, *Phys. Rev. D* **84**, 126001 (2011).
- [19] M. Bianchi and M. Firrotta, DDF operators, open string coherent states and their scattering amplitudes, *Nucl. Phys.* **B952**, 114943 (2020).
- [20] A. Addazi, M. Bianchi, M. Firrotta, and A. Marciandò, String memories ... lost and regained, *Nucl. Phys.* **B965**, 115356 (2021).
- [21] A. Aldi and M. Firrotta, String coherent vertex operators of Neveu-Schwarz and Ramond states, *Nucl. Phys.* **B955**, 115050 (2020).
- [22] A. Aldi, M. Bianchi, and M. Firrotta, String memories... openly retold, *Phys. Lett. B* **813**, 136037 (2021).
- [23] A. Aldi, M. Bianchi, and M. Firrotta, Spinning-off stringy electro-magnetic memories, *Nucl. Phys.* **B974**, 115625 (2022).
- [24] M. Firrotta and V. Rosenhaus, Photon emission from an excited string, *J. High Energy Phys.* **09** (2022) 211.
- [25] Y. Y. Atas, E. Bogomolny, O. Giraud, and G. Roux, Distribution of the Ratio of Consecutive Level Spacings in Random Matrix Ensembles, *Phys. Rev. Lett.* **110**, 084101 (2013).
- [26] F. J. Dyson, Statistical theory of the energy levels of complex systems. II, *J. Math. Phys. (N.Y.)* **3**, 157 (1962).
- [27] P. J. Forrester, *Log-Gases and Random Matrices (LMS-34)* (Princeton University Press, Princeton, NJ, 2010), [10.1515/9781400835416](https://doi.org/10.1515/9781400835416).
- [28] P. Di Francesco, P. Mathieu, and D. Senechal, *Conformal Field Theory*, Graduate Texts in Contemporary Physics (Springer-Verlag, New York, 1997), [10.1007/978-1-4612-2256-9](https://doi.org/10.1007/978-1-4612-2256-9).
- [29] P. H. Ginsparg, Applied conformal field theory, in *Les Houches Summer School in Theoretical Physics: Fields, Strings, Critical Phenomena* (1988), [arXiv:hep-th/9108028](https://arxiv.org/abs/hep-th/9108028).
- [30] J. Cardy, Conformal field theory and statistical mechanics, in *Les Houches Summer School: Session 89: Exact Methods in Low-Dimensional Statistical Physics and Quantum Computing* (2008), [arXiv:0807.3472](https://arxiv.org/abs/0807.3472).
- [31] M. Bianchi, D. Consoli, and J. F. Morales, Probing fuzzballs with particles, waves and strings, *J. High Energy Phys.* **06** (2018) 157.
- [32] M. Bianchi, D. Consoli, A. Grillo, and J. F. Morales, The dark side of fuzzball geometries, *J. High Energy Phys.* **05** (2019) 126.
- [33] P. Erdős and J. Lehner, The distribution of the number of summands in the partitions of a positive integer, *Duke Math. J.* **8**, 335 (1941).
- [34] A. Odlyzko, Tables of zeros of the riemann zeta function, https://www-users.cse.umn.edu/~odlyzko/zeta_tables/.
- [35] A. M. Odlyzko, The 10^{22} -nd zero of the Riemann zeta function, in *Dynamical, Spectral, and Arithmetic Zeta Functions (San Antonio, TX, 1999)*, Vol. 290 of *Contemp. Math.* (American Mathematical Society, Providence, RI, 2001), pp. 139–144, [10.1090/conm/290/04578](https://doi.org/10.1090/conm/290/04578).
- [36] K. Hashimoto, Y. Matsuo, and T. Yoda, Transient chaos analysis of string scattering, *J. High Energy Phys.* **11** (2022) 147.
- [37] J. Polchinski and M. J. Strassler, Hard Scattering and Gauge/String Duality, *Phys. Rev. Lett.* **88**, 031601 (2002).
- [38] M. Bianchi, M. Firrotta, J. Sonnenschein, and D. Weissman, Partonic behavior of string scattering amplitudes from holographic QCD models, *J. High Energy Phys.* **05** (2022) 058.
- [39] O. Fukushima and K. Yoshida, Chaotic instability in the BFSS matrix model, *J. High Energy Phys.* **09** (2022) 039.
- [40] M. Bianchi, A. Grillo, and J. F. Morales, Chaos at the rim of black hole and fuzzball shadows, *J. High Energy Phys.* **05** (2020) 078.
- [41] M. Bianchi, D. Consoli, A. Grillo, and J. F. Morales, Light rings of five-dimensional geometries, *J. High Energy Phys.* **03** (2021) 210.
- [42] F. Bacchini, D. R. Mayerson, B. Ripperda, J. Davelaar, H. Olivares, T. Hertog, and B. Vercoocke, Fuzzball Shadows: Emergent Horizons from Microstructure, *Phys. Rev. Lett.* **127**, 171601 (2021).
- [43] E. Berti, V. Cardoso, and A. O. Starinets, Quasinormal modes of black holes and black branes, *Classical Quantum Gravity* **26**, 163001 (2009).
- [44] G. Aminov, A. Grassi, and Y. Hatsuda, Black hole quasinormal modes and Seiberg–Witten theory, *Ann. Henri Poincaré* **23**, 1951 (2022).
- [45] M. Bianchi, D. Consoli, A. Grillo, and J. F. Morales, More on the SW-QNM correspondence, *J. High Energy Phys.* **01** (2022) 024.
- [46] G. Bonelli, C. Iossa, D. P. Lichtig, and A. Tanzini, Exact solution of Kerr black hole perturbations via CFT2 and instanton counting: Greybody factor, quasinormal modes, and Love numbers, *Phys. Rev. D* **105**, 044047 (2022).
- [47] M. Bianchi, D. Consoli, A. Grillo, and J. F. Morales, QNMs of branes, BHs and fuzzballs from quantum SW geometries, *Phys. Lett. B* **824**, 136837 (2022).
- [48] M. Bianchi and G. Di Russo, 2-charge circular fuzz-balls and their perturbations, [arXiv:2212.07504](https://arxiv.org/abs/2212.07504).
- [49] S. H. Shenker and D. Stanford, Black holes and the butterfly effect, *J. High Energy Phys.* **03** (2014) 067.
- [50] J. Polchinski, Chaos in the black hole S-matrix, [arXiv:1505.08108](https://arxiv.org/abs/1505.08108).

-
- [51] E. J. Martinec and N. P. Warner, The harder they fall, the bigger they become: Tidal trapping of strings by microstate geometries, *J. High Energy Phys.* **04** (2021) 259.
- [52] B. Fristedt, The structure of random partitions of large integers, *Trans. Am. Math. Soc.* **337**, 703 (1993).
- [53] R. Arratia and S. DeSalvo, Probabilistic divide-and-conquer: A new exact simulation method, with integer partitions as an example, *Comb. Probab. Comput.* **25**, 324 (2016).